Technical Memorandum No. 33-230

Characteristics and Format of the Tracking Data to Be Obtained by the NASA Deep Space Instrumentation Facility for Lunar Orbiter

J. Lorell
J. D. Anderson
W. L. Sjogren

JET PROPULSION LABORATORY
CALIFORNIA INSTITUTE OF TECHNOLOGY
PASADENA, CALIFORNIA

June 15, 1965

Technical Memorandum No. 33-230

Characteristics and Format of the Tracking Data to Be Obtained by the NASA Deep Space Instrumentation Facility for Lunar Orbiter

J. Lorell
J. D. Anderson
W. L. Sjogren

T. W. Hamilton, *Manager*
Systems Analysis Section

JET PROPULSION LABORATORY
CALIFORNIA INSTITUTE OF TECHNOLOGY
PASADENA, CALIFORNIA

June 15, 1965

Prepared Under Contract No. NAS 7-100
National Aeronautics & Space Administration

CONTENTS

TABLES

TABLES (Cont'd)

FIGURES

FOREWORD

This document presents information concerning the Deep Space Instrumentation Facility (DSIF) tracking data format and characteristics. It is intended as an explanatory supplement for users of the data to explain the meaning of the data, the locations of the instruments, the biases, the precision and accuracy, the reduction to geometrical quantities, and the format for distribution.

I. INTRODUCTION

With the launching of the Langley Lunar Orbiter, the first opportunity for detailed study of the moon's gravity field will be at hand. Project plans call for concentrated radio tracking by the NASA JPL-operated Deep Space Net (DSN) for a period of several months after the primary (photographic) mission. The resulting information will be made available to the scientific community.

The present document is intended to describe the anticipated data in enough detail to enable recipients of the data to understand it, where it came from, how it was generated, its precision, the noise sources, and the biases. Various options available to recipients range from raw data through refined compressed data to orbit elements as a function of time. Some of the processing procedures that JPL uses are described.

The tracking plan for the Lunar Orbiter was written to support the selenodesy objectives, constrained by the requirements of the primary (photographic) mission. There will be three phases of the coverage. Phase I, corresponding to the duration of the photographic mission, is expected to last about one month. Tracking coverage during this period will be essentially continuous (when the spacecraft is visible from earth), but the data may be degraded by the effect of maneuvers in support of the photography. The second phase starts with the end of the photographic mission and lasts for about one month. Coverage during this phase will be less intensive than in phase I, but yet good enough to ensure sufficient data for detailed gravity studies. Phase III coverage extends from the end of phase II to one year from launch. Coverage during phase III will be at the rate of about seven orbits per week from any station, and should be very effective in identifying long period effects. Specifications of the tracking coverage are given in Section II.

Since the DSN will be responsible for tracking, the data will be received at the DSN tracking stations and transmitted[1] to the Space Flight Operations Facility (SFOF) at JPL for processing and distribution. Qualified scientists will be given access to the data.

Data thus made available may be in various forms, at the option of the requestor. So-called raw data, i.e., data with a minimum of processing, will be provided in the form described in Section III. Such data consists of cumulative doppler count and light seconds as measured by the instruments. Instrument biases are calibrated out; environmental biases are not.

Users will have the option of obtaining clean data—i.e., data processed to some extent to remove biases, or data that has been smoothed by orbit-fitting. For example, range and range-rate values at the observation times could be a requested data form. Another alternative might be the values of the osculating Kepler elements at every tenth observation time. Such processed data and the corresponding format will be made available subject to negotiation and agreement between JPL and the requestor.

Lunar Orbiter tracking data will be both S-band doppler data and range data from the Mark I ranging system. The doppler data are recorded as a cumulative cycle count. Doppler and ranging accuracies are expressed in Section II for "guaranteed" and "probable" cases. Users of the data may wish to perform their own precision analysis on the basis of internal consistency and noise.

Some users may not want all the data, since the volume will be very large. Such users should request compressed data of some form—which may be, for example, the selection of every tenth data point. To understand what will be provided in this case, one should note that the nominal sample spacing for Lunar Orbiter doppler data is one minute (see Sections III and IV). Data compression can be effected by using longer count time, e.g. 10 min. Still longer count times are possible, but probably will result in loss of information.

Ranging is tied in with the doppler signal in the sense that the precision of a range fix depends on the subsequent doppler count. Furthermore, range values at later times, but prior to a new code acquisition, are obtained by doppler count. A reasonable rate of new range fixes is two per hour. Further compression of such data will probably not be desired.

Users are likely to be concerned with the quality of the data. The quality of raw data is indicated in Section II. The quality of processed data will depend, of course, on both the quality of the raw data and the type of processing. Generally, there will be statistics associated with processed data, such statistics providing a measure of its

[1]Data will be transmitted by teletype during the mission and sent by air transport for post-flight analysis.

quality. For example, the statistics could be in the form of a covariance matrix, or as a set of variances together with a correlation matrix.

Uncertainties in the data, of which the statistics are a measure, appear for a variety of reasons, which are basically of two categories, noise and biases. Those sources which produce a randomness in the data[2] are referred to as noise sources. The mathematical representation of these sources for purposes of anlyzing the data is referred to as the noise model. This is useful for both weighting the data and describing its precision. The JPL noise model for doppler data is described in Section V.

Biases represent incorrect parameter values and result in systematic distortion of the data. If a mathematical model is available, it can be used in conjunction with statistical procedures to remove the biases, and thus get better values for the corresponding parameters. Errors in station locations or errors in gravity constants fall into this category. Section VI discusses how improved values for some of these quantities have been obtained using *Ranger* and *Mariner* tracking data. This information is included here to provide the user of the Lunar Orbiter data with the best parameter values so far available.

The method of computing observables in the JPL Orbit Determination Program is described in Section VII. Included here are methods of accounting for light time and refraction.

Finally, Sections VIII, IX, and X provide a description of the DSIF and its capabilities, which should be useful background information.

[2] As exhibited in the scatter of Fig. 5.

II. DEEP SPACE NETWORK COMMITMENT FOR THE LUNAR ORBITER PROJECT

Tracking coverage, guaranteed accuracies, and facilities commitments of the Deep Space Network for the Lunar Orbiter Project[3] are specified in JPL EPD 243 (Ref. 1); the following information is obtained from this document.

1. The Johannesburg (South Africa), Woomera (Australia), Echo (Goldstone, Calif.), Madrid (Spain), and Cape Kennedy (Florida) stations of the DSIF are assigned to support the Lunar Orbiter Project.

2. The DSIF stations assigned to Lunar Orbiter will provide the following coverage at S-band frequencies:

Phase	Coverage
Transit	24 hours/each earth day[4]
If lunar orbit is achieved:	(a) Continuous coverage during all periods in which the spacecraft is visible from the earth for 30 days
	(b) Five consecutive lunar orbits/earth week from any DSIF station supporting the Lunar Orbiter Project for one year
If lunar orbit is not achieved:	24 hr/day for no more than three earth days after encounter and 8 hr/day for not more than an additional ten earth days

3. The DSN will provide raw tracking data and other information to the project for the determination of the orbital parameters of the spacecraft from parking orbit injection to the end of the mission with the following accuracy:
   (a) Angular data.
   Tracking Accuracy, $1\sigma = 0.14$ deg.[5]

[3] For the original LOPO specifications, see pp. 320, 320.1 of Ref. 2.

[4] Except for the Johannesburg site; coverage will be provided to the project for the first pass over the site after launch terminating approximately 12 hr after launch.

[5] This is the equivalent uncorrelated error for one minute sample spacing and represents the specification the DSIF expects to meet for Lunar Orbiter. The sample rate is a meaningful parameter of the statistics but is not necessarily the sample rate contemplated for an actual flight mission. The accuracy of the DSN doppler data (for one minute sampling) depends on signal/noise ratio and spacecraft tumbling characteristics. For favorable S/N ratio and an attitude stabilized spacecraft, rms noise should be well below 0.0015 m/sec. *Effective* noise will be somewhere between 0.0015 m/sec and 0.012 m/sec, with the latter figure being quite pessimistic.

(b) Doppler Data.
Accuracy,[5] $1\sigma = 0.2$ cps $= 0.012$ m/sec.
(c) Ranging Data.
Accuracy,[6] $1\sigma = 15$ m.

4. Tracking Data Monitoring.
The DSN will, in near real time, monitor the quality of the tracking data obtained by the DSIF for the purposes of:
(a) Ensuring that the quality of the tracking data provided to the project meets the specification given in paragraph 3, and
(b) Monitoring DSIF station performance.

The DSN will notify the LOPO whenever the tracking data supplied to the project does not meet the accuracies stated in paragraph 3.

Subsequent to the publication of Ref. 1, the selenodesy requirements for tracking were reviewed, and the requirements updated. The new specifications are detailed in Ref. 3, from which the following is excerpted.

It is suggested that the following principles be adopted with respect to the selenodetic experiment:

1. The selenodesy phase be divided into two phases: S to S+30 days and the balance (S = the end of photo transmissions). Relatively dense tracking would characterize the first phase.
2. During the first phase, i.e., S to S+30 days, continuous tracking over several consecutive orbits would be required to reduce station clock synchronization error effect on accuracy.
3. Coverage from stations committed to the Lunar Orbiter Project with wide latitude separations would be required in the first phase.
4. Provision be made to negotiate more efficient coverage in flight if required. For example, times will exist when the omniantenna nulls are pointing toward the earth, hence coverage would not be required.

Assuming the mission profile to remain as presently designed, i.e., a lunar orbit period of 4 hr or less, the following coverage requirements are proposed:

Interval	Coverage
S to S+30 days	4 orbits per day from any station.
S+30 to L+1 year	7 orbits per week from any station.

It is proposed that the following statement of accuracy requirements be adopted:

Class	Doppler[7]	Ranging[8]
I	0.020 m/sec	15 m
II	0.0005 m/sec	1 m
III	0.0001 m/sec	1 m

It is the opinion of the DSN that the Class I requirement will meet the primary experimental objective and, if met, the Class II requirement would allow the detection of numerous additional harmonics.

The tracking requirements in the SIRD (Ref. 2) are currently in the process of being revised in accordance with the above specifications.

[6]Commitment applied providing spacecraft transponder has ≤ 0.03 μsec delay uncertainty.

[7]Equivalent noise at 1 sample/min.

[8]Sum of high frequency noise plus bias.

III. DATA FORMAT[9]

The raw data will be available on a magnetic tape in the decimal format described in this Section.

A. Long Form

The format of the long form is:

LONG FORM:

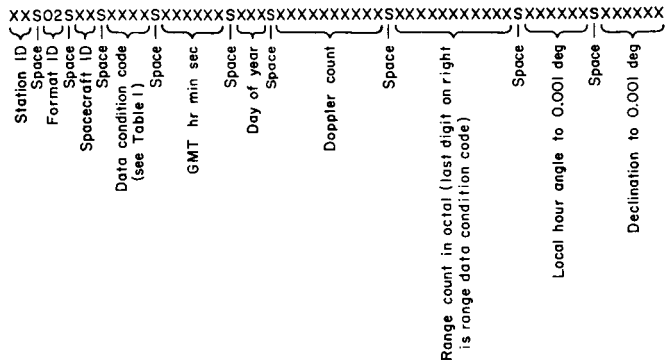

B. Short Form

The short form has the same format as the long form except that the format ID is "03" and there is no hour angle and declination printout. Other format ID's pertain to obsolete systems (L and L-S).

C. Time

The time tag is given in Greenwich mean time (GMT) as transmitted from local WWV time standards (i.e., Hawaii via ionosphere to Woomera). Synchronization of all stations should be well within $\pm$ 10 millisec, and records are kept of periodic checks on time. With the use of ranging data during Lunar Orbiter photographic mission, synchronization may well be within $\pm$ 50 μsec.

D. Doppler

Figure 1 is a simplified diagram of the two-way doppler system. The stable reference oscillator is the heart of the two-way doppler system, for upon return of the signal and the subtraction of the original signal the doppler tone is directly obtained. The doppler sample as

[9]The material in Sections III, IV, V, and VI has been adapted from internal JPL sources by W. L. Sjogren. Also, cf. Ref. 4.

Table 1. Data condition code used by the DSIF stations

Digit No. 1 Doppler averaging time	
Value of digit	**Time**
0	1 sec
1	5 sec
2	10 sec
3	20 sec
4	30 sec
5	40 sec
6	50 sec
7	60 sec
8	Nondestructive or continuous

Digit No. 2 Receiver and servo data condition	
Value of digit	**Data condition**
0	Good doppler and angle data
1	Bad angle data, auto sense
2	Bad doppler data, auto sense
3	Bad doppler and angle data, auto sense
4	Not used
5	Bad angle data, manual switch
6	Bad doppler data, manual switch
7	Bad doppler and angle data, manual switches

Digit No. 3 Doppler mode		
Value of digit	**Counter recorded**	**Doppler mode**
0	1	Two-way (C_2)
1	1	One-way (C_1)
2	1	Two-way two-station noncoherent (C_3)
3	1	Two-way two-station coherent (Cc_3)
4	2	Two-way (C_2)
5	2	One-way (C_1)
6	2	Two-way two-station noncoherent (C_3)
7	2	Two-way two-station coherent (Cc_3)

Digit No. 4 Atomic frequency standard	
Value of digit	**Condition**
0	In lock
1	Out of lock
2	Not applicable

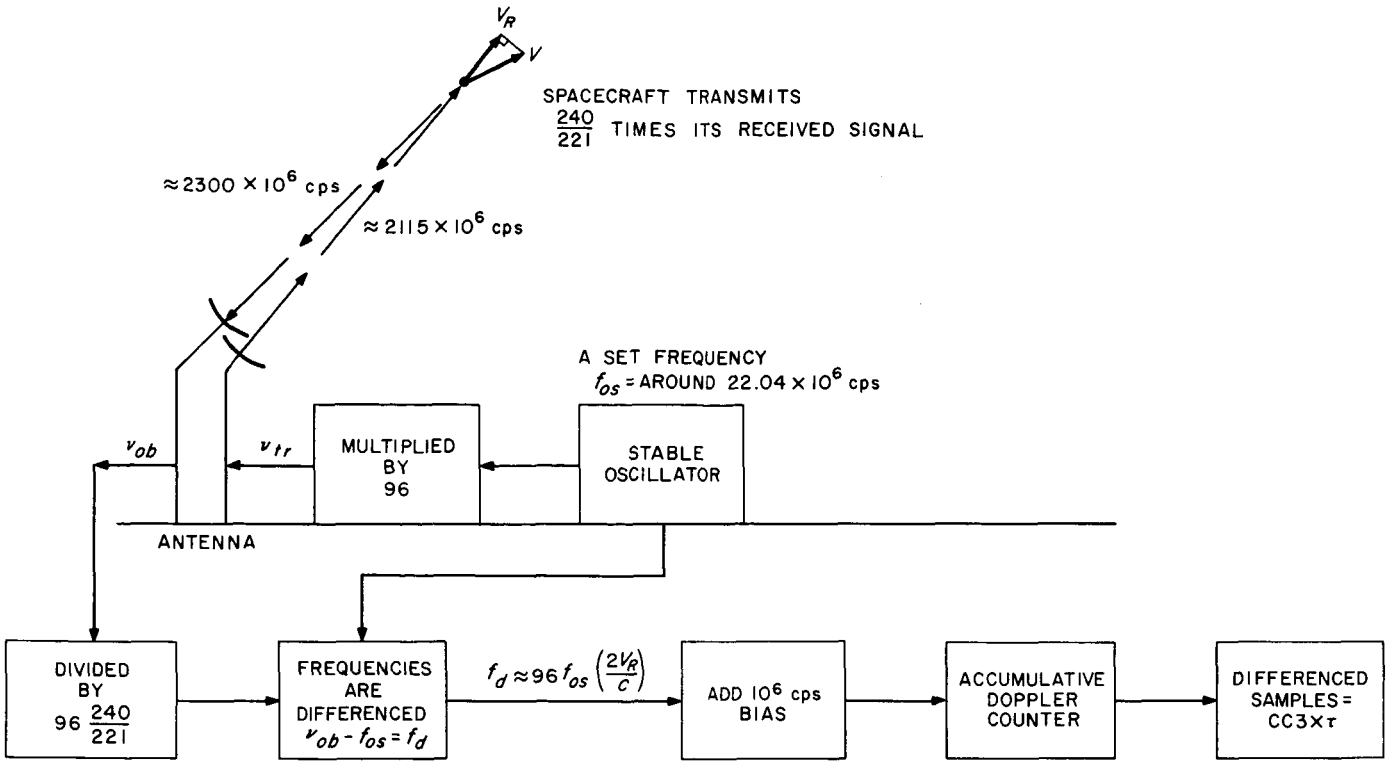

Fig. 1. Simplified two-way doppler system

given by the preceding format is an accumulative counter reading. Two successive readings divided by their time tag difference in seconds (i.e., count time τ) is the observable, CC3.[10] The corresponding time tag for CC3 is the time half way between counter readings. To avoid confusion the observable is given the label CC3, whereas the calculated value for this same quantity is labeled f (see Section VII) for it is their difference, the residual (CC3-f), that is important in the analysis.

Before the calculated value can be obtained, the numerical values of the transmitter frequencies (i.e., f_{os}, $\nu_{tr} = 96\ f_{os}$) must be available. These frequencies will be supplied to users as typed listings with corresponding time tags for each station throughout the mission.

[10]CC3 is the abbreviation for coherent counted three-way doppler. Two-way doppler, the available observable, is essentially the same as coherent counted three-way doppler and therefore has the same label. The "three" represents the transmitter, spacecraft and receiver which may all be widely separated as in the case of "non-coherent" three-way doppler, C3 (i.e., Woomera transmitting and Johannesburg receiving). When the transmitter and receiver antennas are connected directly by microwave as are several Goldstone antennas, then coherent counted three-way doppler may be obtained. However, when the transmitter and receiver are at the same antenna, the effective is the same as the microwave connection and two-way doppler is identical to CC3.

Note the one megacycle bias in Eq. (7-4) (i.e., ω_3). This is required because hardware constraints do not permit negative CC3. However, this bias can be stripped from the observable in the data reducing system and another decimal place (or maybe two) of accuracy can be obtained. This is done in the JPL reduction system.

E. Ranging

The ranging observable is given in *octal* format with the last digit a data condition code. If the last digit is 0, the data is good; if 1, the data is bad. No other processing is necessary. This quantity is essentially a count of the number of cycles of a very stable oscillator that have elapsed during the transmission and reception of a coded signal. The *only* independent range points are those obtained *at* lock-up times, all others are perfectly correlated with the doppler data (i.e., lock must be broken before another independent range point is obtained). Again as in the doppler system, the transmitter frequencies (ν_{tr}) and bias (K_R) will be supplied as typed lists, so that calculated values can be obtained.

F. Editing

Although sufficient information is available in this report to process the raw tracking data, there is available

at JPL a preprocessor of the raw data known as the Tracking Data Processor and Orbit Data Generator computer programs which generate a data file in the proper format for the JPL Orbit Determination Program (the raw data format is not acceptable for direct input into the JPL ODP). These programs do a huge amount of bookkeeping work and make it very easy to modify the quantity and types of data to be handled by the Orbit Determination Program. Figures 2 and 3 are simplified flow diagrams of what is done in each of the programs, whereas Ref. 5 gives a complete description. Appendix I of Ref. 5 (also see Ref. 6, p. 130) shows the required format for the JPL ODP if some other preprocessor is used (i.e., this is also the format which will be available to any other ODP if the JPL preprocessor is used).

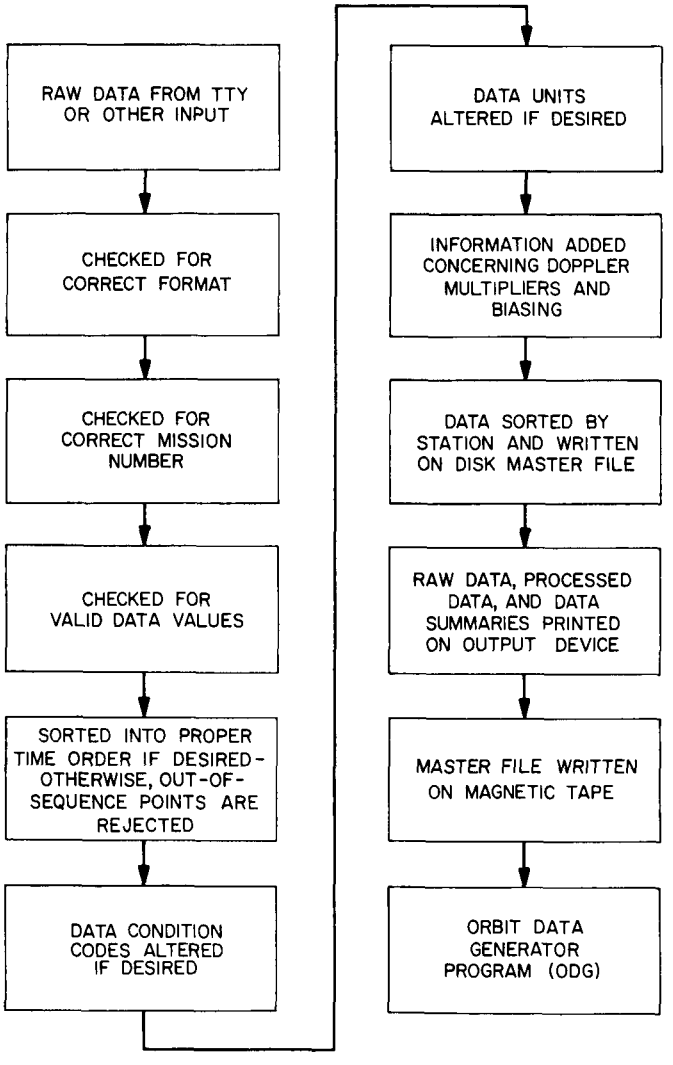

Fig. 2. Simplified flow diagram for Tracking Data Processor (TDP)

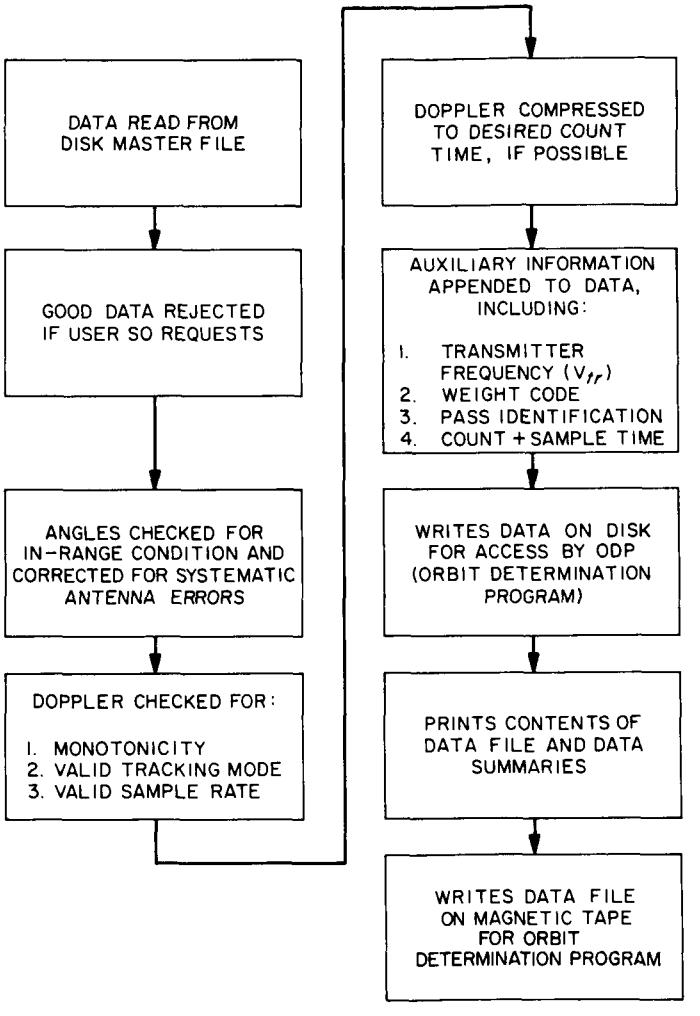

Fig. 3. Simplified flow diagram for the Orbit Data Generator program (ODG)

IV. DATA COMPRESSION

When sampling in the continuous count mode (i.e., mode 3 of Section X-B), there exists the capability of reducing the existing round-off noise and also reducing the number of data points, which could mean a considerable saving in computer running time. However, high frequency and short period effects would be averaged out. Therefore, the initial sample rate should be small enough so that the short period effects can be analyzed, and then this data can be compressed to a much more noise-free data set for analysis of long period parameters. Figure 4 gives some indication of how round-off error is reduced with increased sample count time. At present the maximum compression interval allowable in the JPL Orbit Determination Program is 1023 sec (this software constraint could be changed). There is also the error introduced in the averaging term in the doppler equation which could be cleared up by carrying the higher-order terms (i.e., in Eq. 7-3, add $F^{(IV)}$, $F^{(VI)}$, etc.). However, this would only be necessary where high accelerations exist and other noise sources have been significantly reduced.

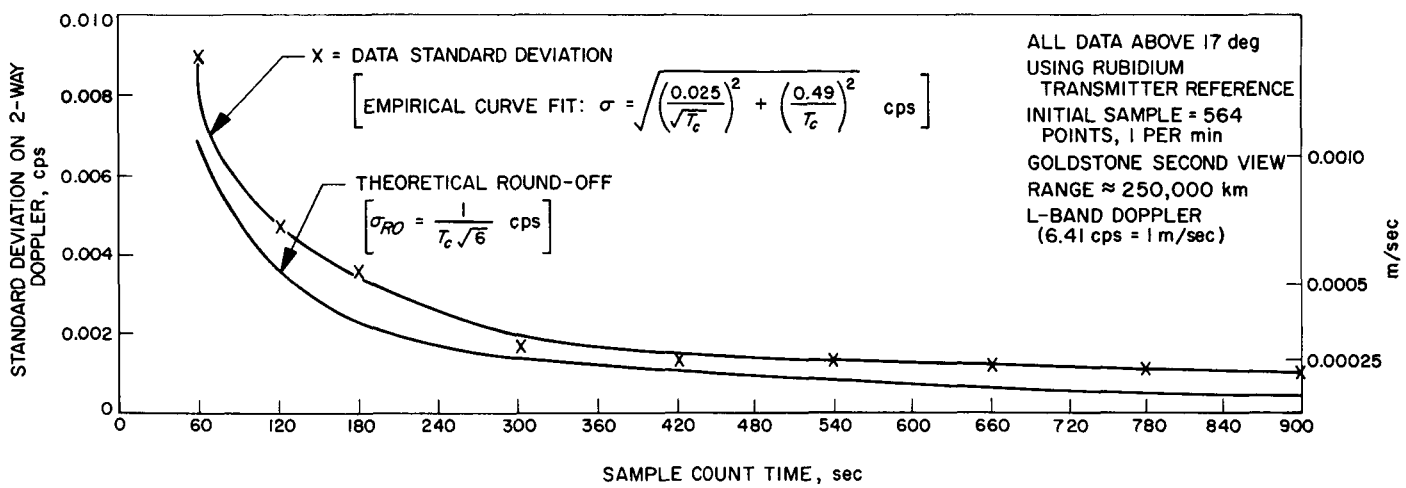

Fig. 4. Standard deviation of *Ranger VII* doppler residuals

V. NOISE MODEL

Although the doppler noise model which is presented here was developed through the analysis of *Ranger* L-band data, it is still applicable to the Lunar Orbiter S-band system. For example, Fig. 5 which is a plot of S-band doppler residuals on *Mariner* Mars has the same characteristics as Fig. 6, which shows the L-band residuals in units of

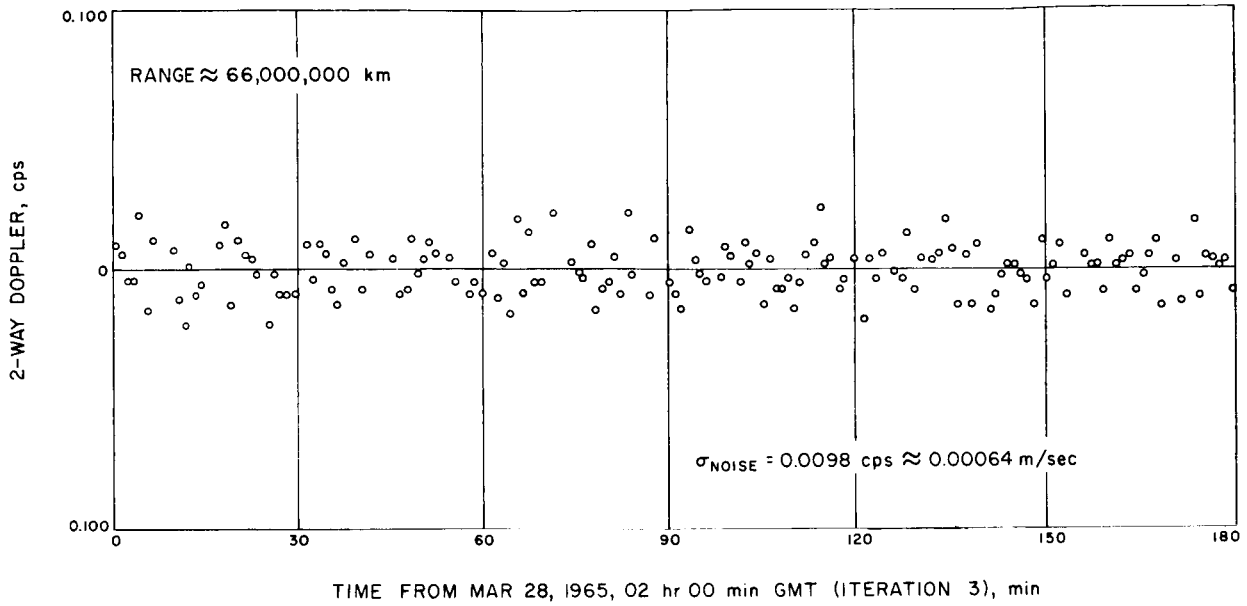

Fig. 5. Goldstone S-band residuals from *Mariner IV* (Mars probe)

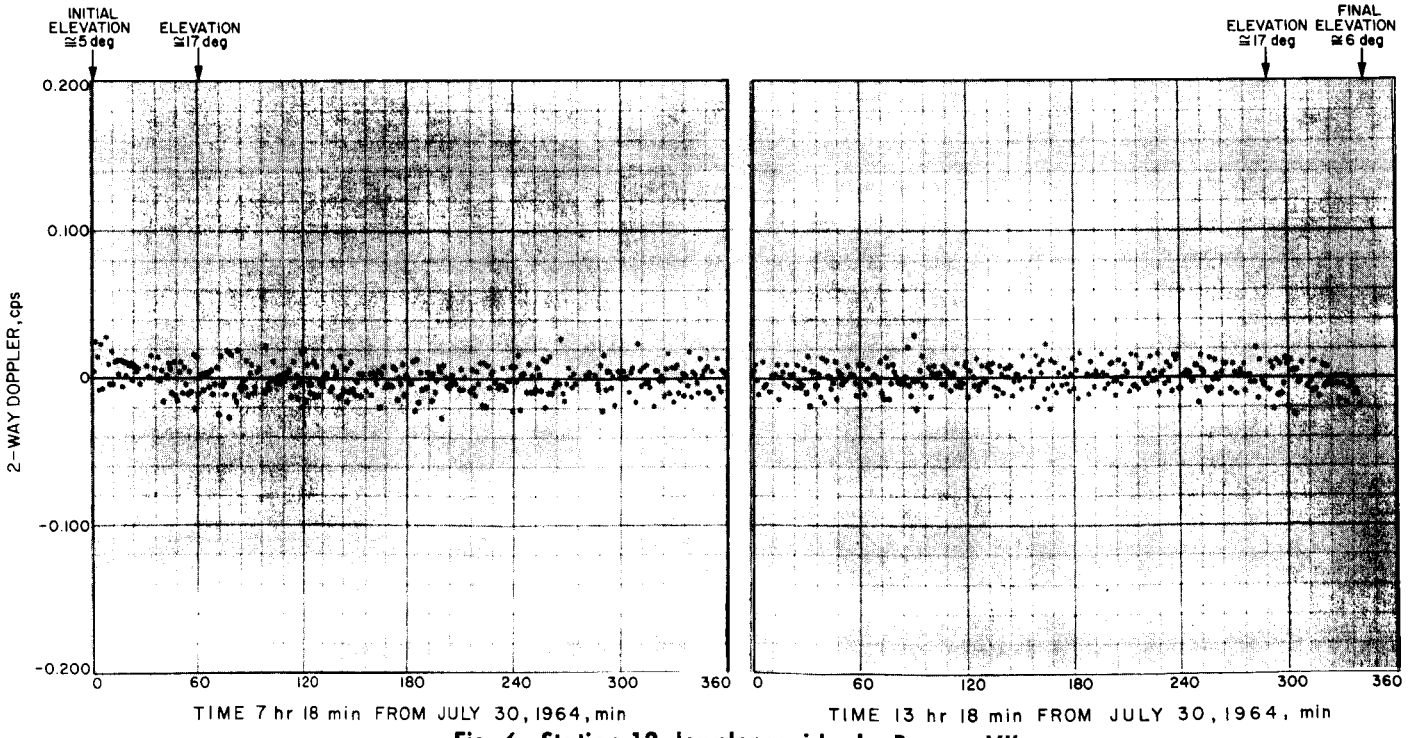

Fig. 6. Station 12 doppler residuals, *Ranger VII*

cycles per second. The following empirical formula was devised to describe the standard deviation of the noise on *Ranger VII* doppler data (its fit is shown in Fig. 4):

$$\sigma(\text{cps}) = \sqrt{(K_1)^2 + \left(\frac{K_2}{\sqrt{T_C}}\right)^2 + \left(\frac{K_3}{T_C}\right)^2}$$

where

T_C = count time

K_1 = 0 cps

K_2 = 0.025 $\text{cps}^{1/2}$

and

K_3 = 0.49 cps

The physical significances of the above terms in the empirical equation are as follows:

1. The K_1 term represents a *frequency* error which is independent of T_C. An example of this type of error is the quantization error due to a finite number of bits available to compute CC3 after the best-fit trajectory has been determined. For the data of Fig. 6, the amplitude of the round-off error in computing the CC3 residual is 6×10^{-5} cps, which is too small to be detected by the empirical curve of Fig. 4.

2. The K_2 term represents a *cumulative count* error which grows as the square root of T_C. Such an error is represented by the cycle drop-out (add-in) behavior which may occur as a result of the receiver phase detector's momentarily losing lock due to excessive phase jitter. The size of K_2 establishes a lower bound on the mean time between these cycle drop-outs (add-ins) of 1600 sec.

3. The K_3 term represents a *cumulative count* error which is independent of T_C. Errors of this type include quantization or round-off error at the doppler counter and phase jitter. The largest component is quantization error. The doppler counters read out the integral number of positive-going zero crossings of the doppler detector output during a preselected time period. This means that the counter reading can differ from the "true count" by up to ± 1 cycle. That is, the count period may start anywhere from just before a zero crossing to just after a zero crossing, which results in a uniform distribution of counter start errors ranging from zero to one count too long. Similarly, the end count error will be a uniform distribution, ranging from zero to one count too short. The net result is a triangular distribution for round-off errors with a standard deviation,

$$\sigma_{\text{quantization}} = \frac{1}{T_C\sqrt{6}} = 0.0068 \text{ cps}$$
$$\text{for } T_C = 60 \text{ sec}$$

The theoretical round-off error curve is included in Fig. 4. Notice that it is the dominant error source below $T_C = 300$ sec.

The appearance of the quantization error in the doppler residuals is isolated in Fig. 7. Actual RA-7 tracking data ($T_C = 1$ sec) is compared to simulated ideal (round-off error only) data for the same time period. The ideal curve was manufactured by simulating by continous-count doppler data with the ODP as it would be generated by the tracking station. These data were then fed back through the ODP, and the resultant residual plot show in Fig. 7 was generated. The slope of the lines depends on the rate of change of the radial velocity. The range rate is increasing at the rate of 0.04 cps in Fig. 4. The slope of the lines will be positive when the range rate is decreasing, and as the rate of change of doppler increases the slope of the lines increases and the lines lose their identity as relatively few residual points fall on any line. The points on the ideal curve all lie between ± 1 cycle of counter error.[11] The actual residuals still fall on the straight lines, but noise other than round-off error may cause a residual in excess of 1 cycle at the counter or may simply cause a point to "shift lines."

After the counter round-off error has been removed from the K_3 term, 0.27 cycle or about 4 cm remain. Such errors are most clearly visible at high sampling rates. Errors of this magnitude can be seen in Fig. 8,[12] which results from an analysis of "N" count[13] data obtained during the *Ranger VII* mission.

[11] In this case, the CC3 residuals lie between ± 1 cps because $T_C = 1$ sec.

[12] Figure 8 is an excerpt from Fig. 1 of a Bisset-Berman Corp. (B-BC) report by H. Epstein (see Ref. 7). Part of the B-BC contract with the NASA Manned Space Center at Houston calls for B-BC to evaluate the potential to the Apollo Project of DSIF-type tracking data. Toward this end, JPL and B-BC cooperate in obtaining and analyzing relevant data.

[13] "N" count is the doppler sampling method in which time is measured for a fixed number of zero crossings (as opposed to the usual procedure of measuring the number of zero crossings for a given time). This method effectively reduces the amplitude of the quantization error for L-band data from 15.6 to 0.8 cm.

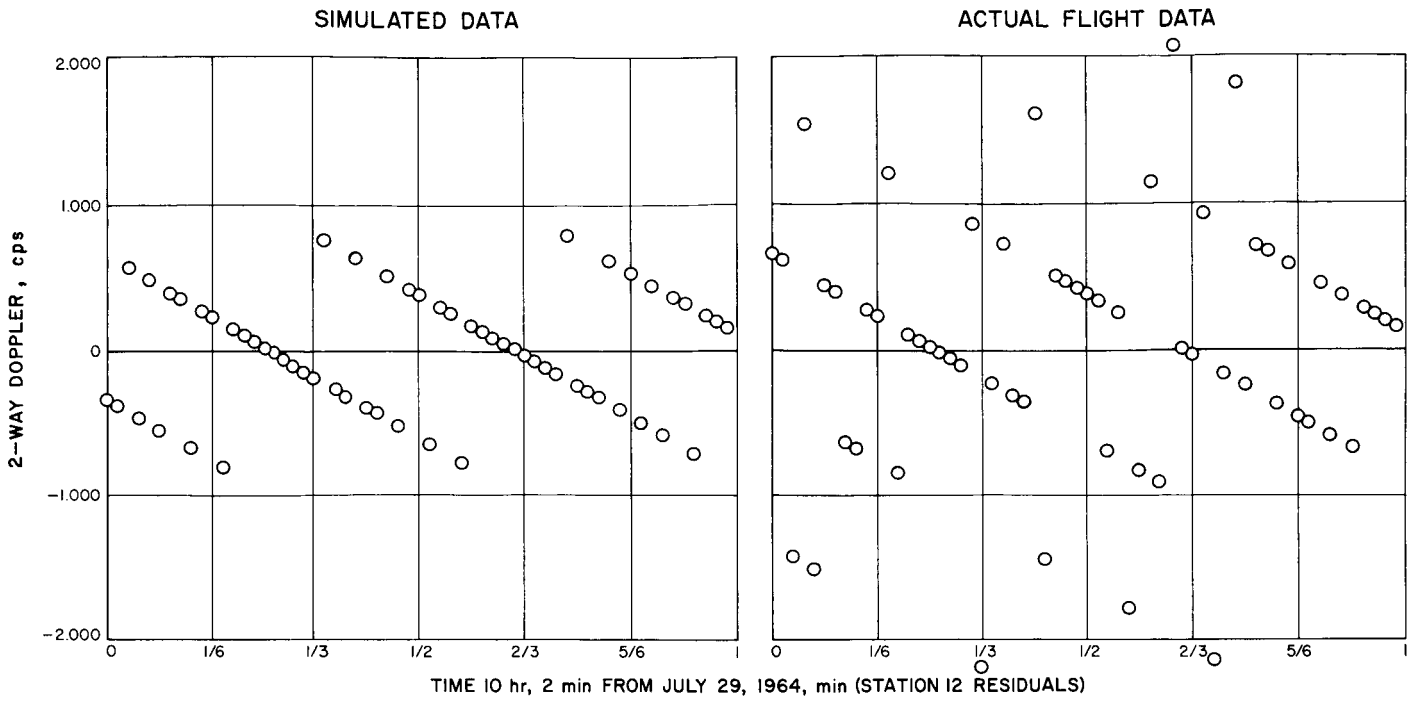

Fig. 7. Quantization error on doppler residuals

A fourth-degree polynomial was fit to 1000-point ($\approx$ 1000 sec) batches of continuous-count data after obvious blunder points (due to teletype format errors, etc.) had been removed. The plot represents residuals in range differences wherein the range difference is taken between the local point plotted and the first point of the batch being analyzed. The 0.8-cm range for quantization errors is relatively small compared with the other data noise. Cycle drop-outs (add-ins) would show up as a 16-cm step in the residuals; no such steps are obvious in Fig. 8. It is currently believed that routine monitoring of critical DSIF frequencies may be responsible for the jumps which are visible in the residuals every 15 min. The jumps are best illustrated on July 31, from 7:45 to 9:05.

The effect of transmitter stability is evident in Fig. 9, which shows the *Ranger VI* two-way doppler residuals from Station 12 in Goldstone. The transmitter VCO crystal was temperature-controlled, and during this pass it had an apparent stability of 2 parts in 10^9. An error is introduced into CC3 which is directly proportional to the net change in the transmitter frequency during the time that the signal is in transit from the transmitter to the spacecraft and back to the receiver. Notice the noise level on the VCO (i.e., off rubidium) visible in Fig. 9 where the range of the spacecraft is approximately 370,000 km, as compared to the rubidium standard. In this case, the round trip time was 2.4 sec and the error of 0.0014 cps (0.00021 m/sec) introduced by the transmitter stability of 5 parts in 10^{11} for $T_c = 60$ sec is negligible compared with the other error sources.

The magnitude of the refraction effect on the doppler data is shown in Fig. 10. These residuals were generated by fitting to the "corrected" data and then passing this trajectory through the data but without the refraction terms included. In practice, the low-elevation doppler is used but is weighted less than high-elevation doppler data. That is, the refraction component of the weighting sigma is proportional to the size of the correction made to the data. This low-elevation doppler strengthens the determination of the tracking station locations.

The most dramatic effect seen in the doppler data is due to the midcourse maneuver. Figure 11 shows the doppler plot for midcourse maneuvers of both *Rangers VI* and *VII*. The heavy continuous line is the predicted curve, and the dots are the actual data points. With the precision doppler, the performance of the maneuver was easily evaluated. In both cases, the difference between the predicted and the total doppler shift was 5 parts in 10^5, or a magnitude less than the expected error in the maneuver *radial* velocity increment.

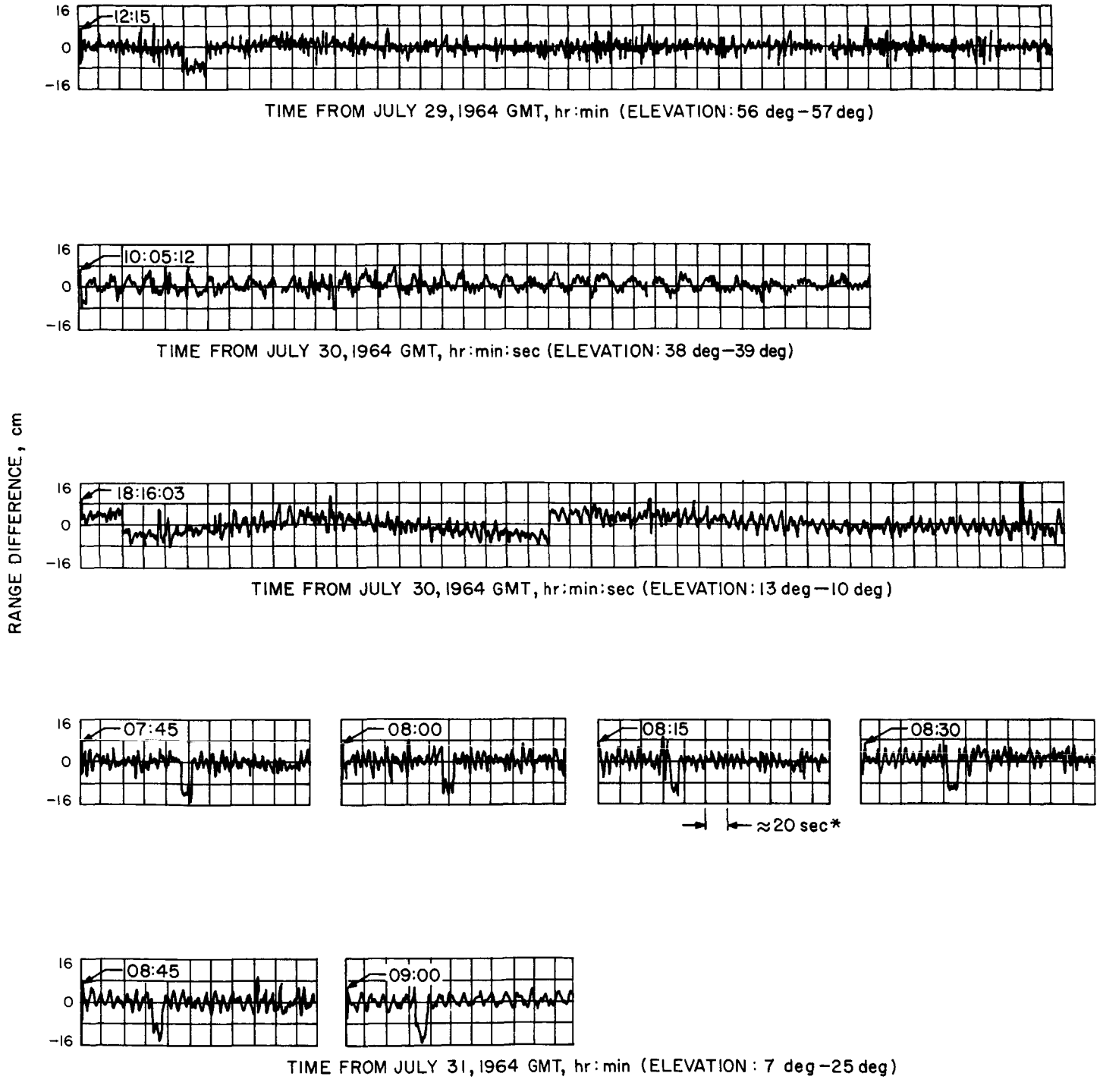

* 20-sec BLOCK IS ACTUALLY THE TIME TO ACCUMULATE 20·(100,000 cycles — THE DOPPLER SHIFT)

Fig. 8. "N" count *Ranger VII* doppler residuals from DSIF station 12

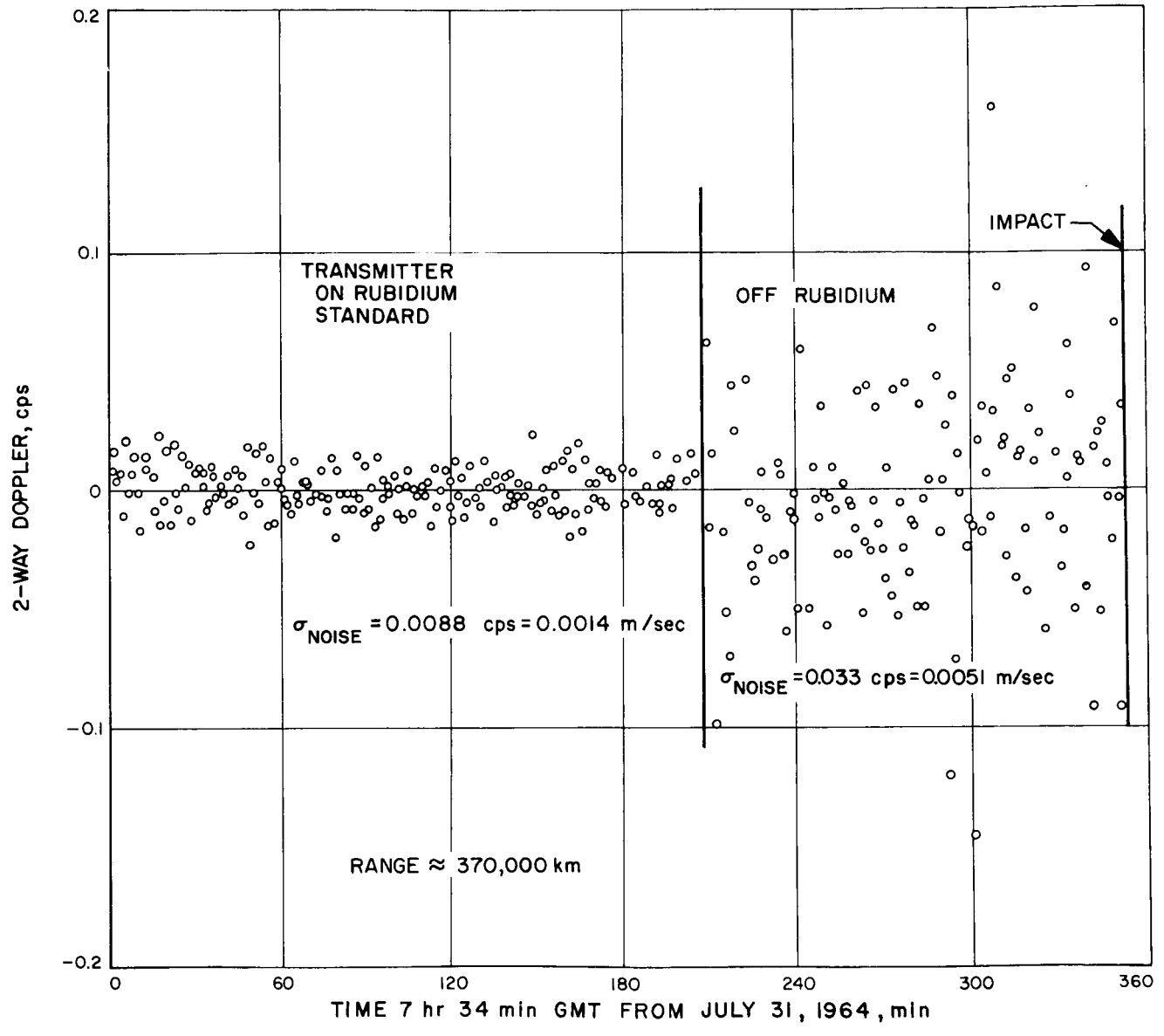

Fig. 9. *Ranger VI* doppler residuals

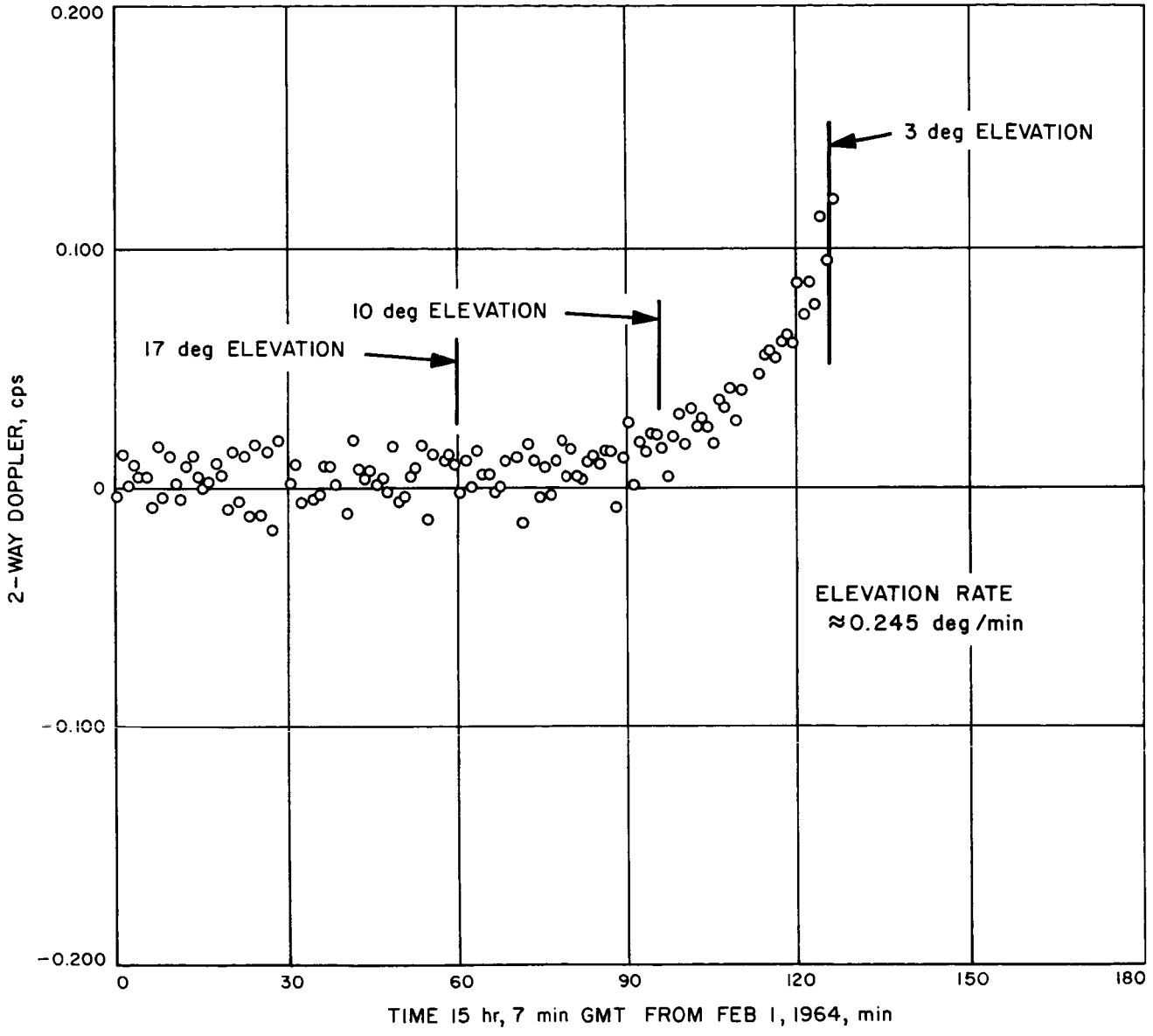

Fig. 10. Effect of refraction in doppler data

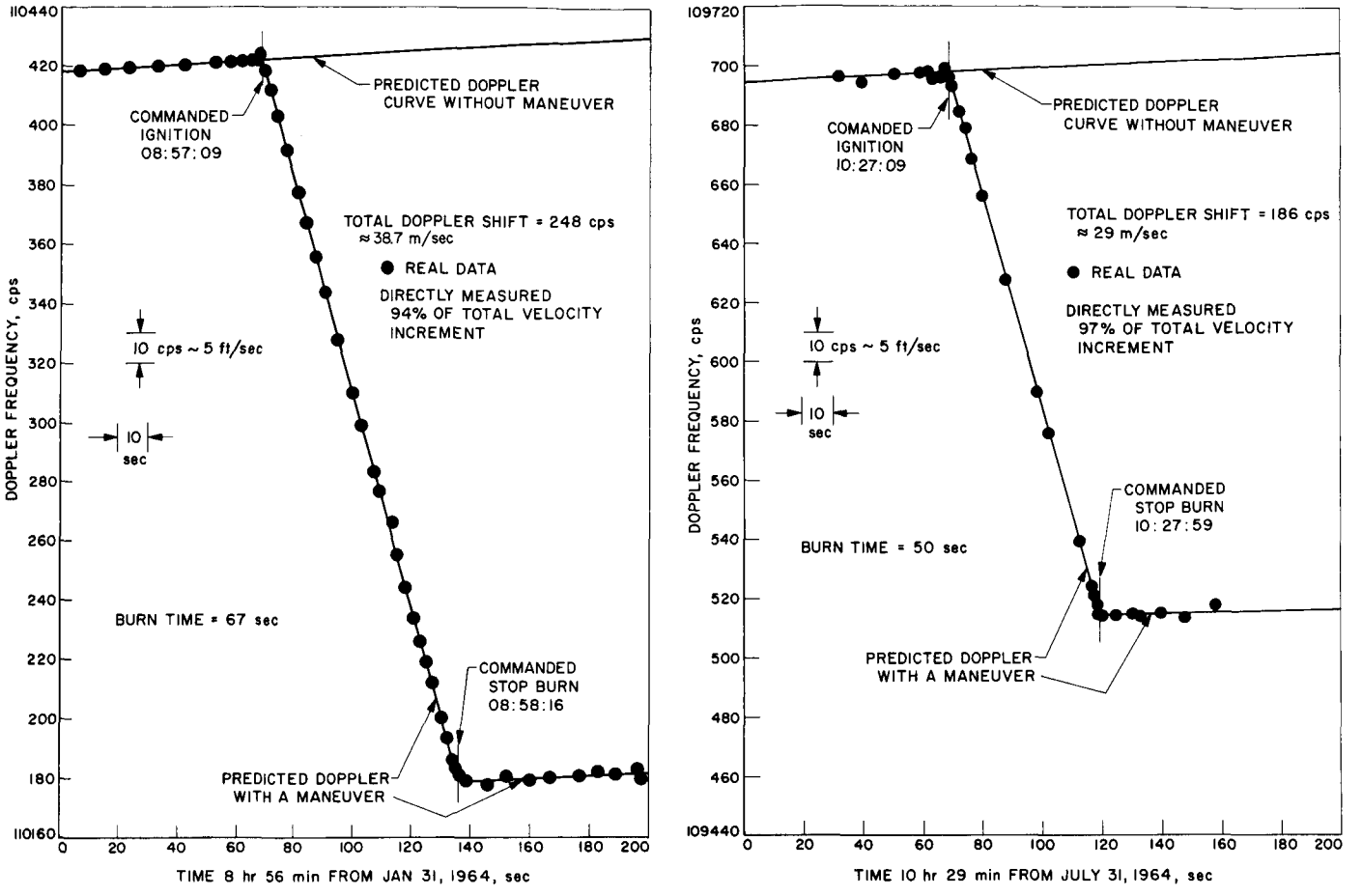

Fig. 11. Doppler data during midcourse maneuvers of *Rangers VI* and *VII*

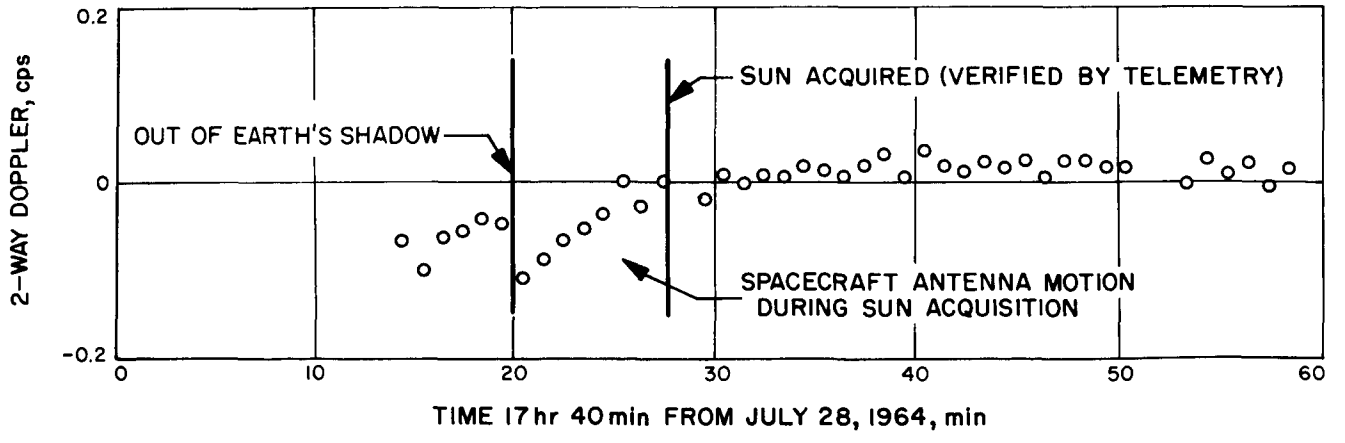

Fig. 12. Doppler residuals during sun acquisition of *Ranger VII*

Spacecraft motion is visible when the spacecraft antenna moves with respect to the spacecraft center of gravity (cg). The ODP estimates the trajectory of the spacecraft cg. A spacecraft rotation about its cg will cause the accumulated counted doppler (which is a range change) to be in error by the net amount that the antenna has been rotated toward (or away from) the tracking station during the accumulation interval. The sun acquisition sequence was visible in the *Ranger VII* doppler residuals shown in Fig. 12. This represents a net range

difference between the antenna and the spacecraft cg of 1.5 m over a period of approximately 240 sec. This time interval is somewhat less than that shown in Fig. 12, because the telemetry time also includes the period needed to damp out oscillations before final lock. The events displayed were all verified by the telemetry data. Prior to acquisition, the spacecraft is tumbling, and this accounts for the noisier data prior to the event.

The *Mariner IV* spacecraft rolled about the sun-line prior to Canopus lock, providing complete 3-axis control. The omniantenna used is at a distance of 36.6 cm from the cg. When the roll period was 30 min, a radial velocity oscillation of 0.12 cm/sec (i.e., 0.0068 cps) was produced (see Fig. 13).

Not only is spacecraft motion detectable in the doppler residuals, but station tracking performance can be seen as well. Figure 14 shows the effect of a timing bias uncovered in the *Ranger VI* data. This was verified when station clock delay times used to synchronize with WWV standards were recalculated and found to be in error. Also, time on telemetry events viewed simultaneously by two stations indicated the same change. The magnitude of the timing error was about 8 msec.

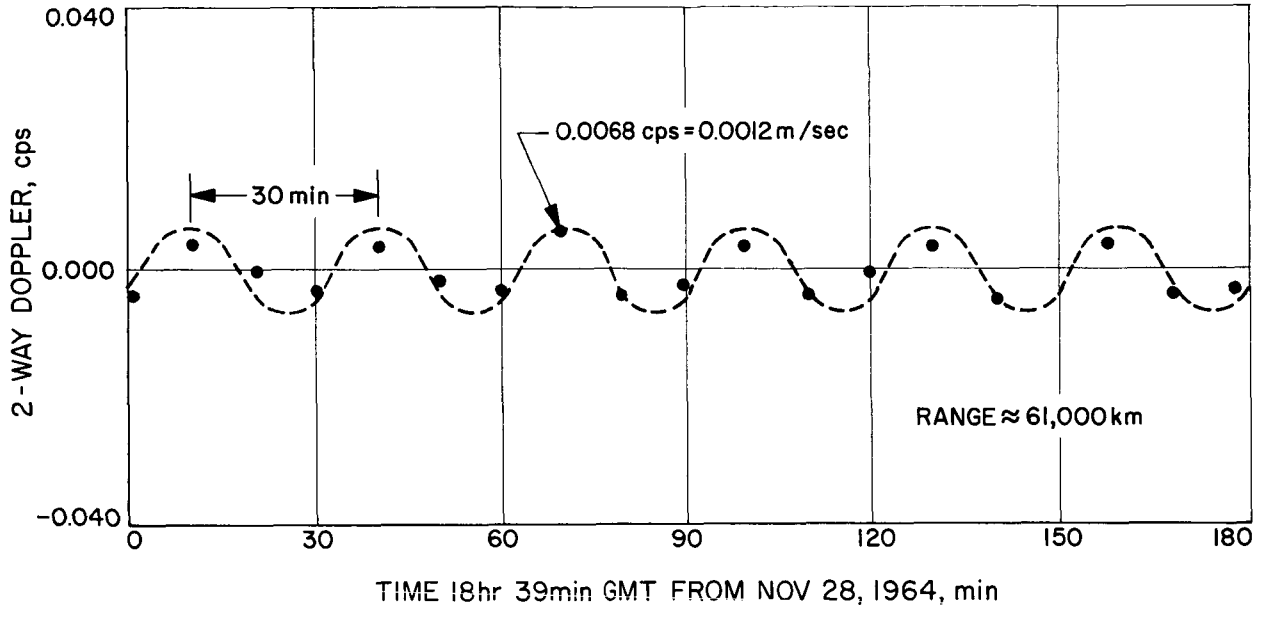

Fig. 13. Effect of Spacecraft motion in station 41 doppler residuals, *Mariner IV*

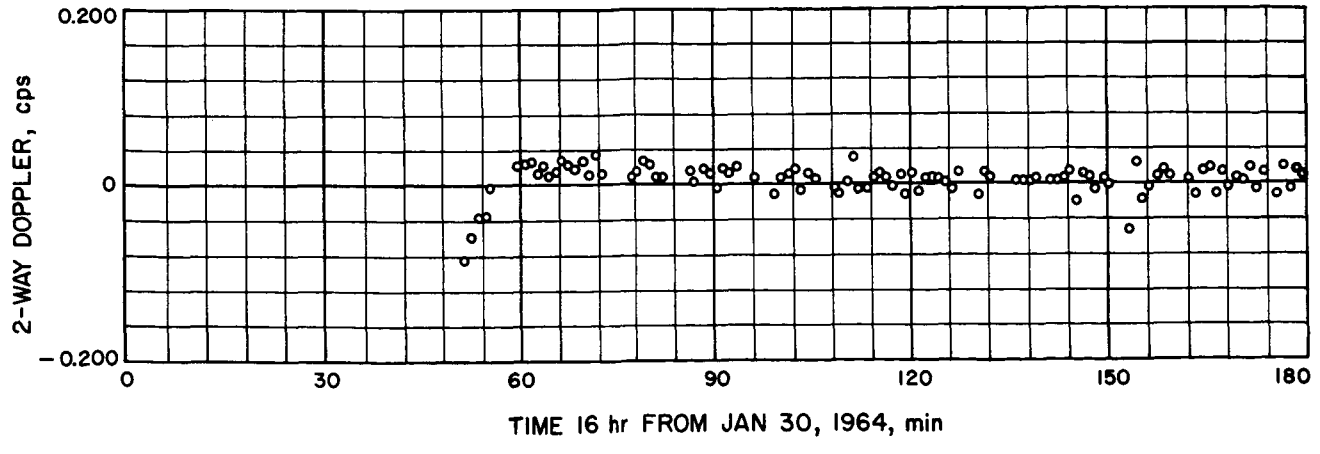

Fig. 14. Effect of timing bias in station 41 doppler residuals, *Ranger VI*

The preceding discussion has been developed directly from the *visible* characteristics in the data. However, in weighting the data to obtain statistics on the estimated parameters, all effects should be accounted for. As a result of this idea, JPL has developed for its orbit determination program a weighting model slightly different from the empirical curve previously given. This model allows for correlations in the data, a priori knowledge of a particular error source, and the capability of adding other noise sources (i.e., spacecraft tumbling).

The expression[14] used to compute the "effective variance" σ^2 for weighting a given data point is

$$\sigma^2 = \sum_{i=1}^{6} s_i^2 \, g_i^2 \, \max\left\{1, \frac{T_{\text{correlation}}}{T_{\text{sample}}}\right\} \qquad (5\text{-}1)$$

where

i = basic error source

$s_i^2 \triangleq$ variance of the basic error source

$g_i^2 \triangleq$ sensitivity coefficient

$T_{\text{correlation}} \triangleq$ correlation width, in seconds, of the basic error source

$T_{\text{sample}} \triangleq$ sample spacing, in seconds

and max a,b means: the larger of the two numbers a, b.

The error sources for two-way doppler are:

1. Errors due to trajectory computations caused by round-off error in the Cowell integrations method.
2. Round-off error caused by the start and stop count pulses not necessarily occurring at times such that an integral number of cycles has passed.
3. Transmitter drift arising from an unstable oscillator. Drift in the voltage controlled oscillator (VCO), which provides the transmitter reference frequency, is 1 part in 10^8 cycles/15 min when not on the rubidium standard, and for the rubidium standard VCO the drift rate is 5 parts in 10^{11} cycles/hr.
4. Dropped or added cycles which are caused by low signal-to-noise ratio where it is possible for the counter to accept a noise pulse as a cycle count.
5. Variation in refraction correction which is due to differences between the atmospheric model used in the calculations and that which actually exists.
6. Spacecraft tumbling caused by antenna motion.

[14]T. W. Hamilton, *Mariner R ODP-TDEP: A Priori Weighting Coefficients*, April 12, 1962 (JPL internal communication).

The physical error sources for hour angle and declination are:

1. Angle jitter in electrical axes or variations about the aiming point caused by the antenna drive mechanism.
2. Angle correction variation which is due to systematic and random variations between the optical and electrical axes.
3. Readout error caused by the encoder system reading out plus or minus one count where one count corresponds to about 0.002 deg.
4. Variation in refraction correction which is due to differences between the atmospheric model which is used and that which actually exists.

Table 2 shows the functional form of the sensitivity coefficients associated with HA, Dec, and two-way doppler. Table 3 presents values of the sensitivity coefficient, variance of the error source, correlation width, and the resulting contribution to the total weight from each assumed basic error source at two different times along the trajectory. The first set was computed for a range of about 55,000 km, and the second set for doppler was computed at a range of about 383,000 km. The second set for angles was computed just before the midcourse maneuver, where the range was about 165,000 km. A nominal sample rate of 60 sec was used to develop Table 3.

Table 2. Sensitivity coefficients, g_i, for hour angle, declination and two-way doppler

Error Source	Sensitivity coefficient		
	HA	Dec	Two-way doppler
1	1/cos (Dec)	1	1
2	1	1	$1/T_c$
3	1	1	ρ ($g = 1$, when $\rho = 400{,}000$ km)
4	Δ_r (HA)*	Δ_r (Dec)*	$1/(3T_c)^{1/2}$
5	0	0	6400 Δ_r ρ*
6	0	0	1

*D. L. Cain, *Refraction Corrections*, July 6, 1960 (JPL internal communication).

Table 3. Contribution from individual error sources to total weight for *Ranger VI* mission[a]

Error source	Early doppler (range = 55,000 km)				Late doppler (range ≈ 383,000 km)			
	g_i^2	s_i^2	Correlation width, sec	σ_i^2 (cps)^2	g_i^2	s_i^2	Correlation width, sec	σ_i^2 (cps)^2
(1) Computing error	1	1.1×10^{-5}	36,000	65.6×10^{-4}	1	1.1×10^{-5}	36,000	65.6×10^{-4}
(2) Rounding error	2.78×10^{-4}	0.16	1	0.5×10^{-4}	2.78×10^{-4}	0.16	1	0.5×10^{-4}
(3) Oscillator drift rate	0.0189	0.41×10^{-2}	600	VCO_T 7.76×10^{-4}	0.917	$(0.41 \times 10^{-2})_{VCO_T}$ $(0.41 \times 10^{-6})_{VCO_R}$	600	$(376.1 \times 10^{-4})_{VCO_T}$ $(0.03761 \times 10^{-4})_{VCO_R}$
(4) Dropped or added cycles	5.56×10^{-3}	0.96	1	5.43×10^{-4}	5.56×10^{-3}	0.96	1	5.34×10^{-4}
(5) Refraction correction	1.11×10^{-6}	0.04	1000	0.007×10^{-4}	3.92×10^{-6}	0.04	1000	0.026×10^{-4}
(6) Spacecraft tumbling	*Zero for Ranger VI*				*Zero for Ranger VI*			
Total	$\sum_{i=1}^{6} \sigma_i^2 = 79.21 \times 10^{-4}$				$\sum_{i=1}^{6} \sigma_i^2 \begin{cases} = (446.6 \times 10^{-4})_{VCO_T} \\ = (71.5 \times 10^{-4})_{VCO_R} \end{cases}$			
	$\sigma = 0.089$				$\sigma \begin{cases} = (0.211)_{VCO_T} \\ = (0.085)_{VCO_R} \end{cases}$			

[a] Sample rate = count time = 60 sec

$$\sigma^2 = \sum_{i=1}^{6} s_i^2 g_i^2 \max \left\{1, \frac{T_{correlation}}{T_{sample}}\right\}$$

Table 3. Contribution from individual error sources to total weight for *Ranger VI* mission[a] (Cont'd)

Error source	Early angles (range ≈ 55,000 km)				Late angles (range ≈ 165,000 km)			
	g_i^2	s_i^2	Correlation width, sec	σ_i^2 (deg)^2	g_i^2	s_i^2	Correlation width, sec	σ_i^2 (deg)^2
(1) Angle jitter in electrical axes	Dec = 1 HA = 1.026	9.0×10^{-6}	1	Dec = 0.09×10^{-4} HA = 0.0924×10^{-4}	Dec = 1 HA = 1.008	9.0×10^{-6}	1	Dec = 0.09×10^{-4} HA = 0.0907×10^{-4}
(2) Angle correction variation	1	1.0×10^{-4}	20,000	333.33×10^{-4}	1	1.0×10^{-4}	20,000	333.33×10^{-4}
(3) Readout error	1	1.44×10^{-6}	1	0.0144×10^{-4}	1	1.44×10^{-6}	1	0.0144×10^{-4}
(4) Refraction correction	Dec = 1.26×10^{-4} HA = 2.48×10^{-4}	4.0×10^{-2}	1000	Dec = 0.84×10^{-4} HA = 1.65×10^{-4}	Dec = 4.12×10^{-4} HA = 2.44×10^{-4}	4.0×10^{-2}	1000	Dec = 2.75×10^{-4} HA = 1.63×10^{-4}
Total				$\sum_{i=1}^{6} \sigma_i^2 = \begin{cases} = (334.27 \times 10^{-4})_{\text{Dec}} \\ = (335.06 \times 10^{-4})_{\text{HA}} \end{cases}$ $\sigma = \begin{cases} = (0.183)_{\text{Dec}} \\ = (0.183)_{\text{HA}} \end{cases}$				$\sum_{i=1}^{6} \sigma_i^2 = \begin{cases} = (336.18 \times 10^{-4})_{\text{Dec}} \\ = (335.06 \times 10^{-4})_{\text{HA}} \end{cases}$ $\sigma = \begin{cases} = (0.183)_{\text{Dec}} \\ = (0.183)_{\text{HA}} \end{cases}$

[a] Sample rate = count time = 60 sec

$$\sigma^2 = \sum_{i=1}^{6} s_i^2 g_i^2 \max \left\{ 1, \frac{T_{\text{correlation}}}{T_{\text{sample}}} \right\}$$

Table 4. Estimates and statistics on DSIF station locations using deep space tracking data[a]

Mission	Coordinate off the earth's spin axis X_1		Coordinate longitude X_2		Difference in longitude			
	Mission-survey, m	Standard deviation, m	Mission-survey, m	Standard deviation, m	Mission-survey, m	Standard deviation, m	Mission-survey, m	Standard deviation, m
	Goldstone, California (12)				$X_{212}-X_{241}$		$X_{212}-X_{251}$	
LAND SURVEY	0	30	0	30	0	37	0	37
MARINER II	−24	30	9	30	—	—	—	—
RANGER VI	−36	10	−18	32	−131	22	23	19
RANGER VII	−35	9	1	31	−140	23	27	18
RANGER VIII[b]	−35	9	−15	30	−133	22	23	20
	Woomera, Australia (41)				$X_{241}-X_{251}$		$X_{241}-X_{212}$	
LAND SURVEY	0	30	0	30	0	37	0	37
RANGER VI	88	38	113	39	154	22	131	22
RANGER VII	65	37	141	37	167	25	140	23
RANGER VIII[b]	75	20	114	30	156	22	133	22
	Johannesburg, South Africa (51)				$X_{251}-X_{212}$		$X_{251}-X_{241}$	
LAND SURVEY	0	30	0	30	0	37	0	37
RANGER VI	−33	19	−41	36	−23	19	−154	22
RANGER VII	−16	21	−26	31	−27	18	−167	25
RANGER VIII[b]	−17	20	−44	30	−23	20	−156	22

[a] Absolute values for station coordinates can be found in Table 6 and in Ref. 8, pg. 14, Table 7, column 8.
[b] Preliminary Result.

(horizon-to-horizon track). Note that the statistics on x_1 at Goldstone are a factor of 3 below the best land surveys and that the statistics in the differences in longitude are also below land surveys. Since rubidium standards will be used at Woomera and South Africa in the near future, these stations will soon be as well determined as Goldstone is now.

Table 5 displays the estimates of the dynamical constants, $GM_\oplus$ and $GM_\leftmoon$, from the *Ranger* and *Mariner* missions.

The solution for $GM_\oplus$ appears to be slightly smaller than that set by the Astronomical Union in Paris in 1963. A value of approximately 398601.2 ± 1.0 seems like a good estimate. The values for $GM_\leftmoon$ are very consistent. Of course, with these estimates of $GM_\oplus$ and $GM_\leftmoon$ and because of the constraint equation containing them, the mean earth–moon distance $A_\leftmoon$ is determined to approximately 350 meters one sigma from the formula

$$A_\leftmoon = 60.2665876\left[86.315745\,(GM_\oplus + GM_\leftmoon)^{1/3}\right]$$

Table 5. Results on $GM_\oplus$ and $GM_\leftmoon$

Source	Value, km^3/sec^2	Standard deviation, km^3/sec^2	Remarks
	GM_{Earth} estimates = $GM_\oplus$		
Nominal JPL[a]	398603.20	± 4.0	4 days of tracking
Ranger III	398600.49	± 4.1	4 days of tracking
Ranger IV	398601.87	±13.3	8 hr of tracking
Ranger V	398599.20	±13.2	8 hr of tracking
Ranger VI	398600.61	± 1.1	65 hr of tracking
Ranger VII	398601.28	± 1.5	68 hr of tracking
Ranger VIII[b]	398601.23	± 0.7	65 hr of tracking
	GM_{Moon} estimates = $GM_\leftmoon$		
Nominal JPL (Prior to *Mariner* '62)	4900.7589	± 5.0	
Nominal JPL[a] (After *Mariner* '62)	4902.7779	± 0.3	Venus cruise data taken during Mariner '62
Ranger VI	4902.6182	± 0.14	65 hr of tracking
Ranger VII	4902.5801	± 0.17	68 hr of tracking
Ranger VIII[b]	4902.6435	± 0.12	65 hr of tracking

[a] Value set by Symposium 21, International Astronomical Union, Paris, 1963.
[b] Preliminary result.

The doppler data type at present requires the use of two weight codes. One code is used when the tracking station is not using the rubidium standard for the transmitter frequency voltage controlled oscillator $(VCO)_T$, and the other code is used when the station is using the rubidium standard $(VCO)_R$, which is about three magnitudes more stable than the $(VCO)_T$.

Early in the mission the predominant error sources affecting doppler are the computing error (error source 1), oscillator drift (error source 3), dropped or added cycles (error source 4), and possibly refraction correction (error source 5), depending on the elevation angle rate. As the mission progresses, the oscillator drift rate becomes the sole predominant error source if the station is using the $(VCO)_T$, but if the station is using $(VCO)_R$ this error source contributes a relatively negligible amount to the total weight. For example, near encounter where the contribution from this error source is a maximum, the error attributed to oscillator drift rate for the $(VCO)_R$ is $\sigma^2 = 0.03756 \times 10^{-4}$, and for the $(VCO)_T$ it is $\sigma^2 = 375.6 \times 10^{-4}$.

For the angular data types (HA, Dec), the predominant source of error is angle correction variation (error source 2). Angle jitter may contribute heavily to HA for declination angles near 270 or 90 deg. The contribution due to refraction correction was relatively small and was essentially cut off for elevation angles greater than 17 deg.

It is felt that the total weight applied to HA, Dec, and CC3 is on the conservative side and that all error sources which contribute a measurable amount to the total weight have been taken into account. It should be noted, however, that the large contribution of error source 1 on doppler (computing error) is due to the Single Precision Orbit Determination Program and this will be greatly reduced when the Double Precision Program (now in development) becomes available.

VI. ACCURACY OF STATION LOCATIONS AND DYNAMICAL CONSTANTS

Station locations can be estimated with tracking data quite well in two coordinates, but very poorly in the third. The coordinate system which best suits station location estimation using space probe data is a station-fixed rectangular system (Fig. 15). The x_1 axis is normal to the earth's spin axis, passing through the station in the station meridian plane. The x_2 coordinate is similar to longitude. It is normal to x_1 and to the earth's spin axis. The third coordinate, x_3 is parallel to the earth's spin axis. The x_1 and x_2 components are well determined from the tracking data, whereas x_3 is only partially determined. In general, when horizon-to-horizon tracking is available, x_1 can be determined to within 10 m, and the difference in longitude between two stations can be obtained to 20 m. Although x_3 cannot be estimated practically and its uncertainty may be as large as 300 m, its effect on the solution orbit for any lunar or interplanetary space probe is small.

Table 4 displays the station location results from *Rangers VI, VII,* and *VIII* and *Mariner II* as deviations from a "best" land survey.[15] Note the consistency in the differences. Station 12, Goldstone, has the best estimates, since it has the rubidium standard and consequently has been allowed to accumulate much more tracking data

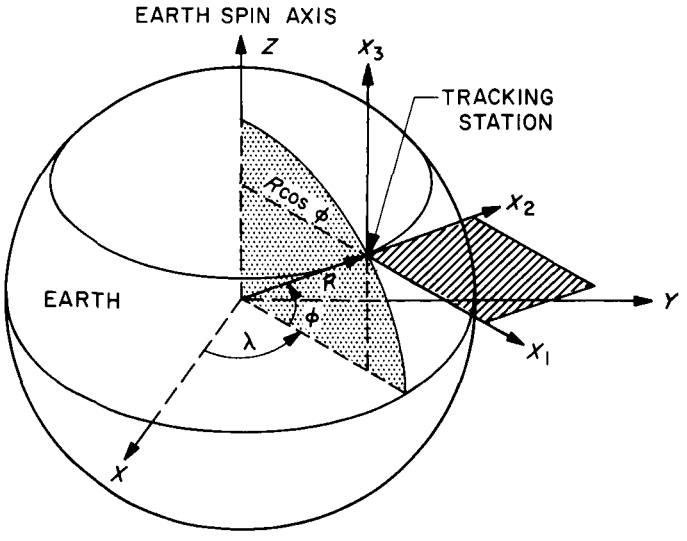

Fig. 15. Coordinate system for estimating station location with deep space tracking data

[15]For station locations, see Section IX, Table 6.

VII. COMPUTATION OF OBSERVABLES

A. Mathematical Model for Doppler Data

This section describes the method used at JPL to interpret the doppler data in terms of the dynamical model. Thus it becomes possible to form residuals in the data and to apply standard statistical techniques taken from the theory of parameter estimation. The approach is to leave the actual data fundamentally unaltered and to construct a mathematical model which accounts for all the properties of the data. To this end it is necessary to understand the nature of the observational equipment and the propagation of the electromagnetic signal in space and in the earth's atmosphere. It should be noted that an alternative approach, not considered here, is to process the data such that it is reduced to a form which admits a fairly simple mathematical representation, for example, instantaneous range or range rate. Then the description of the equipment and the propagation properties are included in a data reduction before the application of the estimation procedure.

Doppler data obtained in the radio region of the electromagnetic spectrum are generated by counting the number of cycles that occur in an interval of time τ. For example, a signal sent from the spacecraft is received at the antenna and a cycle count device determines the number of cycles in the signal for the interval τ by recording the number of zero crossings of the incoming wave. Such a system is called a one-way doppler system. For the actual DSIF data, called two-way doppler, a signal of known constant frequency is transmitted to the spacecraft which in turn returns the signal to a receiver on the ground. By using atomic frequency standards the transmitted frequency can be held to something of the order of five parts in 10.[11] The signal at the spacecraft is multiplied by a constant k before it is returned to earth. The errors introduced into the signal by the transponder in the spacecraft are negligible.

In any cycle count system the important quantity is the signal that enters the cycle count device. A mathematical representation of the cycle count over a finite interval is achieved by first considering the number of cycles in this signal that occur in an infinitesimal interval. Let the number of cycles that occur in an interval of time t to $t + dt$ be given by dn. Then if $F(t)$ represents the number of cycles per unit time inherent in the signal, it is permissible to write

$$dn = F(t)\,dt \tag{7-1}$$

The number of cycles that occur over a finite time τ is obtained by integrating Eq. (7-1). By convention the data are identified by a time of observation t_{ob} at the end of the count interval. Also the number of cycles in interval $t_{ob} - \tau$ to t_{ob} is divided by τ to normalize the cycle count and give it units of frequency (cps). The resulting observable is designated[16] f and is given by

$$f = \frac{1}{\tau}\int_{t_{ob}-\tau}^{t_{ob}} F(t)\,dt \tag{7-2}$$

The integral is evaluated numerically by computing $F(t)$ and its second derivative at the midpoint t_m of the count interval ($t_m = t_{ob} - \frac{1}{2}\tau$). The resulting approximation to the frequency f is

$$f = F(t_m) + \frac{\tau^2}{24}\ddot{F}(t_m) \tag{7-3}$$

The approximation becomes worse as τ is increased.

It remains to specify the function $F(t)$ for the DSIF two-way doppler. Let the transmitted frequency be ν_{tr} and the observed frequency be ν_{ob}. Then the function $F(t)$ is

$$F(t) = \omega_3 + \omega_4 \nu_{tr}\left(1 - \frac{\nu_{ob}}{\omega_4 \nu_{tr}}\right) \tag{7-4}$$

where ω_3 and ω_4 are constants[17] peculiar to the mechanization of the doppler equipment.

The ratio $\nu_{ob}/\omega_4\nu_{tr}$ is derived in terms of the relative position and velocity of the station and the spacecraft by standard techniques. Designate the range and range rate at time of transmission of the signal by $\rho_{(tr)}$ and $\dot{\rho}_{(tr)}$, respectively, and at time of observation of the signal by $\rho_{(ob)}$ and $\dot{\rho}_{(ob)}$, respectively, and the velocity of light by c. Then the result is

$$\frac{1}{\omega_4}\frac{\nu_{ob}}{\nu_{tr}} = 1 - \frac{\dot{\rho}(tr) + \dot{\rho}(ob)}{c} + \frac{1}{c^2}\left[\dot{\rho}(ob)\,\dot{\rho}(tr) + \dot{\rho}^2(ob) + H\right] \tag{7-5}$$

[16] Cf. Section III, where f = theoretical calculated doppler, CC3 = observed doppler.

[17] $\omega_3 = 10^6$ cps, $\omega_4 = 240/221$, $\nu_{tr} = 96\ f_{os}$ (cf. Fig. 1) c = velocity of light = 299792.5 km/sec.

where, in terms of the position vectors **r** and **R** defined below,

$$H = \mathbf{r}(tp) \cdot \left[\frac{\dot{\rho}(ob)}{\rho(ob)} \dot{\mathbf{R}}(t;\, rec) - \frac{\dot{\rho}(tr)}{\rho(tr)} \dot{\mathbf{R}}(t_{tr};\, tr) \right] + \frac{1}{2} \left[\dot{R}(t;\, rec) \cdot \dot{R}(t;\, rec) - \dot{R}(t_{tr};\, tr) \cdot \dot{R}(t_{tr};\, tr) \right] \tag{7-6}$$

Terms of order $1/c^3$ are not included in the ratio and relativistic terms of order $1/c^2$ and above are also neglected. The quantities in Eq. (7-5) and (7-6) are computed from the position $r(t_p)$ of the spacecraft at time t_p when it receives the signal sent from the transmitter at position $\mathbf{R}(t_{tr};\, tr)$ and time t_{tr}. Also the position $\mathbf{R}(t;\, rec)$ of the receiver at the time t when it receives the signal is required, as are the time derivatives of the three positions. All positions and velocities are geocentric.

The range $\rho(tr)$ and range rate $\dot{\rho}(tr)$ for the transmitter are computed by

$$\rho^2\,(tr) = \left[r(tp) - \mathbf{R}(t_{tr};\, tr) \right] \cdot \left[r(tp) - \mathbf{R}(t_{tr};\, tr) \right] \tag{7-7}$$

and

$$\rho(tr)\,\dot{\rho}(tr) = \left[r(tp) - \mathbf{R}(t_{tr};\, tr) \right] \cdot \left[r(tp) - \dot{\mathbf{R}}(t_{tr};\, tr) \right] \tag{7-8}$$

The expressions for the receiver are similar. All coordinates **R** and $\dot{\mathbf{R}}$ for the two stations are given as a function of the time and the location of the stations on the earth. The coordinates **r** and $\dot{\mathbf{r}}$ of the spacecraft are obtained as a function of time by numerically integrating the equations of motion for the spacecraft.

Equations (7-5), (7-6), (7-7), and (7-8) completely specify ν_{ob}/ω_{4tr} as a function of time t. The additional times t_p and t_{tr} are computed by means of the light time correction described in Section VII-B for a given value of t. The function $F(t)$ is now available through the substitution of Eq. (7-5) into Eq. (7-4), but the observable f cannot be computed from Eq. (7-3) without a value of $F(t)$. This value is obtained by twice differentiating Eq. (7-5). For this purpose the $1/c^2$ term is neglected. Then

$$\ddot{F}(t) = \frac{\omega_4\, \nu_{tr}}{c} \left[\ddot{\rho}(t_{tr}) + \rho(t_{ob}) \right] \tag{7-9}$$

where $\ddot{\rho}$ is obtained by twice differentiating Eq. (7-8).

Now $F(t)$ and $\ddot{F}(t)$ can be evaluated at the known time $t_m = t_{ob} - \frac{1}{2}\tau$, and the representation of the cycle count data is complete for the case of an earth with no atmosphere. The corrections for light time and atmospheric refraction are discussed in Section VII-B.

To calculate the range observable use the following formula with the previously described notation:

$$R = \frac{\omega_4\, \nu_{tr} \left[(\rho_{tr}) + \rho(_{ob}) \right]}{16c} + \epsilon \qquad \text{in cycles} \tag{7-10}$$

where

$$\epsilon = K_R\, (16c/\omega_4\, \nu_{tr})$$

K_R = a constant for a station and a view period

B. Corrections to Computed Cycle Count

Two corrections enter into the representation of the doppler data. The first of these, the light-time correction, is applied to obtain the unknown times t_p and t_{tr} from the known time t. The resulting three times are used in the computation of range and range rate for the receiver and transmitter. The second correction accounts for the passage of the radio signal through the atmosphere. A static exponential atmosphere is assumed and ionospheric effects are neglected. The S-band frequencies are high enough to permit the exclusion of the ionosphere, at least within the accuracy of the approximate atmospheric model.

In applying the refraction correction, it is the computed values of cycle count that are modified; the data are left as is.

1. Light-Time Correction

The light time correction is concerned with relating three event times so that the range and range rate vectors from the transmitter to the probe and from the receiver to the probe can be represented accurately. The time of reception of the electromagnetic signal at the station is t, while the time at which the probe sends the signal to the receiver is t_p. A third time is required when a ground transmitter is involved in the system. It is the time of transmission t_{tr}. The reception of a signal at the probe and its transmission by the probe to the ground are assumed to be simultaneous events.

The procedure makes use of a time t'_p which is an approximation to t_p and which is defined by

$$t'_p = t - \frac{1}{c} \left[r(t'_p) - a_e \right] \tag{7-10}$$

where $r(t'_p)$ is the geocentric distance to the probe at time t'_p, a_e is the mean equatorial radius of the earth, and c is the speed of light. Now all quantities required at time t_p are computed at t'_p instead and are then linearly corrected by the time increment $\epsilon_t = t_p - t'_p$.

For example the position vector of the spacecraft at t_p is given by

$$\mathbf{r}_p(t_p) = \mathbf{r}_p(t'_p) + \epsilon_t \dot{\mathbf{r}}_p(t'_p) \tag{7-11}$$

The rigorous light time correction is

$$\Delta t_p = t - t_p \tag{7-12}$$

while the approximate correction is

$$\Delta t = t - t'_p = \frac{1}{c}\left[r(t'_p) - a_e\right] \tag{7-13}$$

Therefore the increment ϵ_t required to correct the quantities evaluated at t'_p is

$$\epsilon_t = \Delta t - \Delta t_p \tag{7-14}$$

and an expression for Δt_p is needed as a function of quantities evaluated at t'_p. The advantage of introducing t'_p in this way is that when iterating on the light time correction to find $\mathbf{r}_p(tr)$, say, the probe ephemeris is entered only once at time t'_p.

The value of Δt_p is determined by the iteration formula

$$\Delta t_p = \frac{\rho + \dot{\rho}\Delta t}{c + \dot{\rho}} \tag{7-15}$$

where ρ and $\dot{\rho}$ are computed from the best available estimate of the position and velocity of the spacecraft at time t_p. The position is computed by Eq. (7-11) with the current estimate of ϵ_t. The velocity is computed by a similar formula.

The time interval $t_p - t_{tr}$ required for the determination of the transmitter coordinates is approximated by setting it equal to the time interval $t - t_p$.

2. Atmospheric Refraction Correction

The correction to the observables caused by the bending of an electromagnetic wave in the atmosphere is somewhat unsatisfying because the atmosphere is not static and fluctuations will cause unknown variable errors in any corrective formula. It is therefore necessary to resort to mean corrections based on some reasonable model of the atmosphere.

The first assumption in deriving the refraction correction is that the wave is confined to a plane containing the observer, the object, and the center of the earth. In other words a signal is sent from P and arrives at S (Fig. 16).

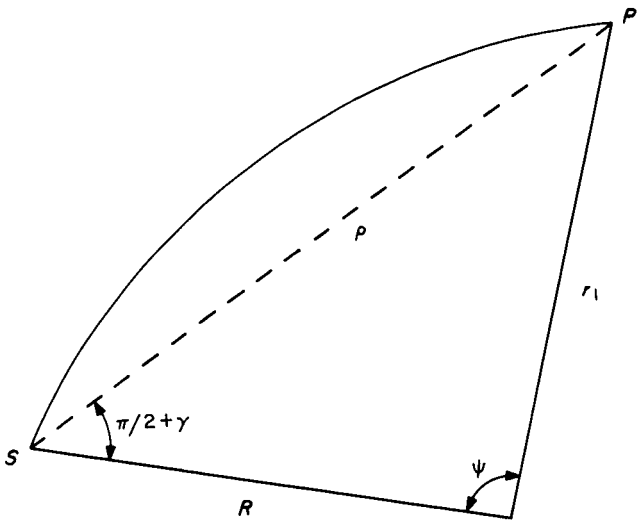

Fig. 16. Refraction geometry

The next assumption is that a ray through the atmosphere will follow the path which makes the time of transmission a minimum. This is Fermat's principle which can be implemented either through the calculus of variations or by applying Snell's law to an infinitesimal shell of the atmosphere and then by integrating over the whole atmosphere. In either case an assumption as to the value of the index of refraction n as a function of position in the atmosphere is required. A spherically symmetric model for n is assumed with an exponential radial dependance.

$$n = 1 + (n_0 - 1)\, e^{-\frac{H}{S}} \tag{7-16}$$

where H is the height above the surface of a spherical earth.

A plot of the correction to range as a function of the observed elevation angle is given in Fig. 17 for a scale height S of 7.315 km and a value of $n_0 - 1$ of 3.40×10^{-4}. For this purpose the range is defined as the propagation time $t - t_p$, or, to put it in length units, as $c\,(t - t_p)$. The correction is for a spacecraft at infinite height, or, effectively, at a point where the earth's atmosphere is negligible.

For purposes of calculation, an empirical interpolation formula for the range correction $\Delta\rho$ is used in place of the actual curve (Fig. 17) generated by numerical integration.

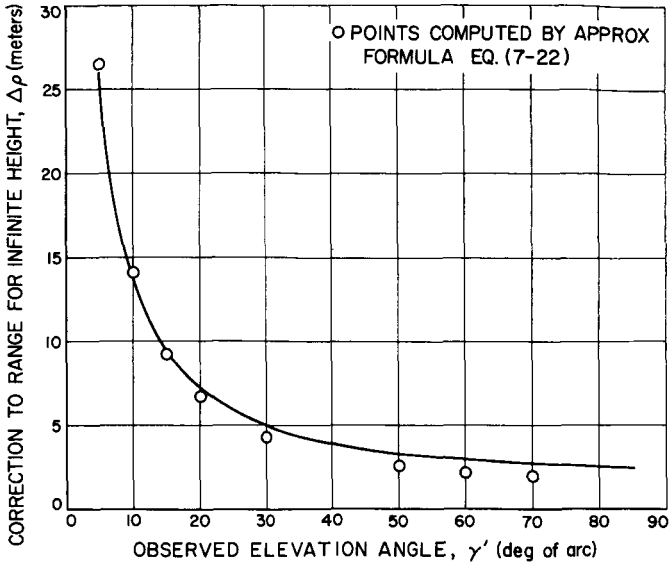

Fig. 17. Range correction for infinite height

That the range curve is all that is required for doppler can be shown by considering Eq. (7-5) to order $1/c$.

$$\frac{1}{\omega_4}\frac{\nu_{ob}}{\nu_{tr}} = 1 - \frac{2\dot{\rho}}{c} \tag{7-17}$$

Then by combining the above with Eq. (7-2) and (7-4) the doppler data are represented to order $1/c$ by the relation

$$f = \frac{1}{\tau}\int_{t_{ob}-\tau}^{t_{ob}} \left[\omega_3 + \frac{2\omega_4 \nu_{tr}}{c}\dot{\rho}\right] dt \tag{7-18}$$

or

$$f = \omega_3 + \frac{2\omega_4 \nu_{tr}}{c\tau}\int_{t_{ob}-\tau}^{t_{ob}} \frac{d\rho}{dt}\, dt \tag{7-19}$$

Therefore an approximate formula for two-way doppler is

$$f = \omega_3 + \frac{2\omega_4 \nu_{tr}}{c\tau}\left[\rho(t_{ob}) - \rho(t_{ob} - \tau)\right] \tag{7-20}$$

The correction Δf is the difference of two range corrections:

$$\Delta f = \frac{2\omega_4 \nu_{tr}}{c\tau}\left[\Delta\rho(t_{ob}) - \Delta\rho(t_{ob} - \tau)\right] \tag{7-21}$$

The interpolation formula used for the range correction is

$$\Delta\rho = \frac{0.0018958}{(\sin\gamma + 0.06483)^{1.4}} \tag{7-22}$$

where γ is the elevation angle of the spacecraft above the station horizon. It can be computed as a function of time from a knowledge of the orbit of the spacecraft. Points computed by the formula (Eq. 7-22) are plotted on Fig. 17 for comparison with the numerically integrated curve.

Finally the refraction correction to f is

$$\Delta f = A\left\{\frac{1}{\left[\sin\gamma\,(t_{ob}) + B\right]^{1.4}} - \frac{1}{\left[\sin\gamma\,(t_{ob} - \tau) + B\right]^{1.4}}\right\} \tag{7-23}$$

where

$$A = (0.0018958)\frac{2\omega_4 \nu_{tr}}{c\tau}$$

and

$$B = 0.06483$$

Again all quantities are evaluated at the midpoint t_m of the count interval, and the elevation angles at each end are approximated by

$$\gamma(t_{ob}) = \gamma(t_m) + \frac{1}{2}\tau\,\dot{\gamma}(t_m) \tag{7-24}$$

and

$$\gamma(t_{ob} - \tau) = \gamma(t_m) - \frac{1}{2}\tau\,\dot{\gamma}(t_m) \tag{7-25}$$

The elevation angle rate $\dot{\gamma}$ is, like γ, evaluated from the orbit of the spacecraft and the position and velocity of the station at t_m.

VIII. DEEP SPACE INSTRUMENTATION FACILITY[18]

The Deep Space Instrumentation Facility (DSIF) is a precision tracking and communications system capable of providing command, control, tracking, and data acquisition from spacecraft designed for deep space exploration. (As used here, "deep space" means distances from the earth of more than 10,000 miles.) Although it is designed for use in deep space exploration, the DSIF may be used with other types of missions wherein its capabilities can be used to advantage.

The DSIF is comprised of seven[19] Deep Space Stations (one under construction), a launch area spacecraft monitoring station, an intersite communications network, and a DSIF operations control center.

The seven Deep Space Stations are located at longitudes approximately 120 deg apart so as to provide continuous coverage of a spacecraft in deep space. Stations are located at Goldstone, California (one under construction); Woomera, Australia; Johannesburg, South Africa; Canberra, Australia; and Madrid, Spain (under construction). The Deep Space Stations are equipped with 85-ft-diameter polar-mount reflector antennas which have maximum tracking rates of 0.7 deg per sec. The spacecraft monitoring station is located at Cape Kennedy, Florida, and is presently equipped for L-band frequencies only. The DSIF Operation Control Center is located at the Jet Propulsion Laboratory, Pasadena, California.

The design philosophy of the DSIF is to provide a precision radio tracking system which measures two angles, radial velocity, and range and to utilize this system for two-way communications with spacecraft in an efficient and reliable manner. The DSIF will be improved and modernized to remain consistent with state-of-the-art and project requirements.

The National Aeronautics and Space Administration is the cognizant agency responsible for the DSIF. The Jet Propulsion Laboratory is under contract to NASA for research, development, and procurement relating to the Deep Space Stations, mobile stations, and monitoring stations and for the technical coordination and liaison necessary to establish and operate the DSIF throughout the world. Overseas Deep Space Stations are generally operated by personnel provided by cooperating agencies in the respective countries. The Goldstone stations and the monitoring station are operated by United States personnel.

In addition to their participation in the DSIF, the Goldstone stations are utilized for extensive investigation into space tracking and communication techniques and for the development of new equipment. In most cases, the new equipment will be installed and tested at Goldstone before it is integrated into the DSIF. Once this equipment has been accepted for general use within the DSIF, it is classed as Goldstone Duplicate Standard (GSDS) equipment, which standardizes the design and formalizes the documentation of like items throughout the net.

Operational control of the DSIF during a mission is provided by the DSIF Control Center, which is located in the Space Flight Operations Facility (SFOF) at JPL. The SFOF furnishes trajectory information to the DSIF, reduces the data which the DSIF acquires from the spacecraft, furnishes command and control data to the DSIF for transmission to the spacecraft, and furnishes facilities for the operations control of spacecraft. The DSIF together with the SFOF and the interstation communication is called the Deep Space Network (DSN).

[18]The material in this section has been adapted from Ref. 9.

[19]A mobile station is presently located near the Johannesburg Deep Space Station. It is primarily used for early tracking and telemetry data from *Ranger* spacecraft using L-band frequencies. It will be dismantled when all of these spacecraft have been launched, which is expected to be not later than July 1965.

IX. STATION GEOMETRY AND COVERAGE[20]

The locations of the Deep Space Stations have been selected to be approximately 120 deg apart in longitude and between 40 deg N and 40 deg S latitude, so that a spacecraft which is more than 10,000 miles away from the Earth will be under continuous surveillance. The locations of all the stations and their antennas are given in Table 6.

The loci of subvehicle points—with 0-deg horizon mask angles employing the 85-ft-diameter polar-mount (hour angle and declination coordinates) antennas at Goldstone, Johannesburg, and Woomera — are shown in Fig. 18; Fig. 19 shows the loci of subvehicle points for an 8-deg horizon mask for Goldstone, Madrid, and Canberra. Figures 18 and 19 indicate the field of view of each polar-mount Deep Space Station as a function of vehicle altitude as well as the region of overlapping coverage.

In the DSIF, it is planned to construct large, 210-ft-diameter parabolic antennas and to locate one of these antennas at each of three selected Deep Space Station sites. The present schedule calls for the first large antenna to be installed at Goldstone by January 1966, the second near Madrid in 1967, and the third near Canberra in 1967. These antennas will be constructed with altazimuth mounts but will employ a Master Equatorial to read out in polar-mount coordinates and will have elevation limits of approximately 5 deg.

The DSIF which has been equipped to communicate with spacecraft at L-band frequencies, (nominal 890 Mc transmit and 960 Mc receive) is presently being converted to S-band (nominal 2100 Mc transmit and 2300 Mc receive) and will become operational at all stations on S-band frequencies during the period from July 1964 to March 1966 (see Table 7).

[20]The material in this section has been adapted from Ref. 9.

Table 7. S-band implementation schedule

Station	Date operationally capable	
	L-S[a]	Full S-band
Goldstone (Pioneer)		operational
Goldstone (Echo)		July 1965
Woomera	September 1964	March 1966
Johannesburg	September 1964	March 1966
Canberra		operational
Madrid		July 1965
Spacecraft monitoring		May 1965

[a]L-S is an interim capability obtained by providing sufficient equipment to receive S-band frequencies on the L-band receiver; IF frequencies and information bandwidths are the same as for the L-band receiver system.

Table 6. Station location[a]

Location	Antenna diameter, ft	Station identification number	Geodetic latitude	Geodetic longitude	Height above mean sea level, meters[b]	Geocentric latitude	Geocentric longitude	Geocentric radius, km
Goldstone, Calif. (Pioneer)	85	11	35.38950N	243.15175E	1037.5	35.20805N	243.15080E	6372.0639
Goldstone, Calif. (Echo)	85	12	35.29986N	243.19539E	989.5	35.11861N[g]	243.19445E[g]	6372.0449[g]
Goldstone, Calif. (Mars [c,d])	210	13	35.24772N	243.20599E	1213.5	35.06662N	243.20505E	6372.2869
Goldstone, Calif. (Venus [e])	85	14	35.42528N	243.12222E	1160	35.24376N	243.12127E	6372.1594
Woomera, Australia	85	41	31.38314S	136.88614E	144.8	31.21236S[g]	136.88614E[g]	6372.5481[g]
Canberra, Australia	85	42	35.40111S	148.98027E	654	35.21962S	148.98027E	6371.6816
Johannesburg, S. Africa	85	51	25.88921S	27.68570E	1409.1	25.73876S[g]	27.68558E[g]	6375.5504[g]
Madrid, Spain [c,d]	85	61	40.429 N	355.751 E	800	40.334 N	355.751 E	6374.37
Spacecraft monitoring, Cape Kennedy, Fla. [f]		71	28.48713N	279.42315E	4.0	28.32648N	279.42315E	6373.2874

[a]The parameters are referenced to the NASA Earth Model Spheroid with an equatorial radius of 6378.165 km and a flattening of 1/298.3; all based on land survey.
[b]Measured to the point of intersection of the hour angle axis with the plane of the declination gear on polar mount antennas.
[c]Under construction with estimated completion as follows: Goldstone, Mars, January 1966; Madrid, June 1965.
[d]Tentative location; definite location to be determined after antenna erection.
[e]This station is used normally for engineering and development; on special assignment it may be used in operations.
[f]Temporary location of present L-band station.
[g]Solutions of these parameters from actual tracking data are given in Ref. 8 and 10.

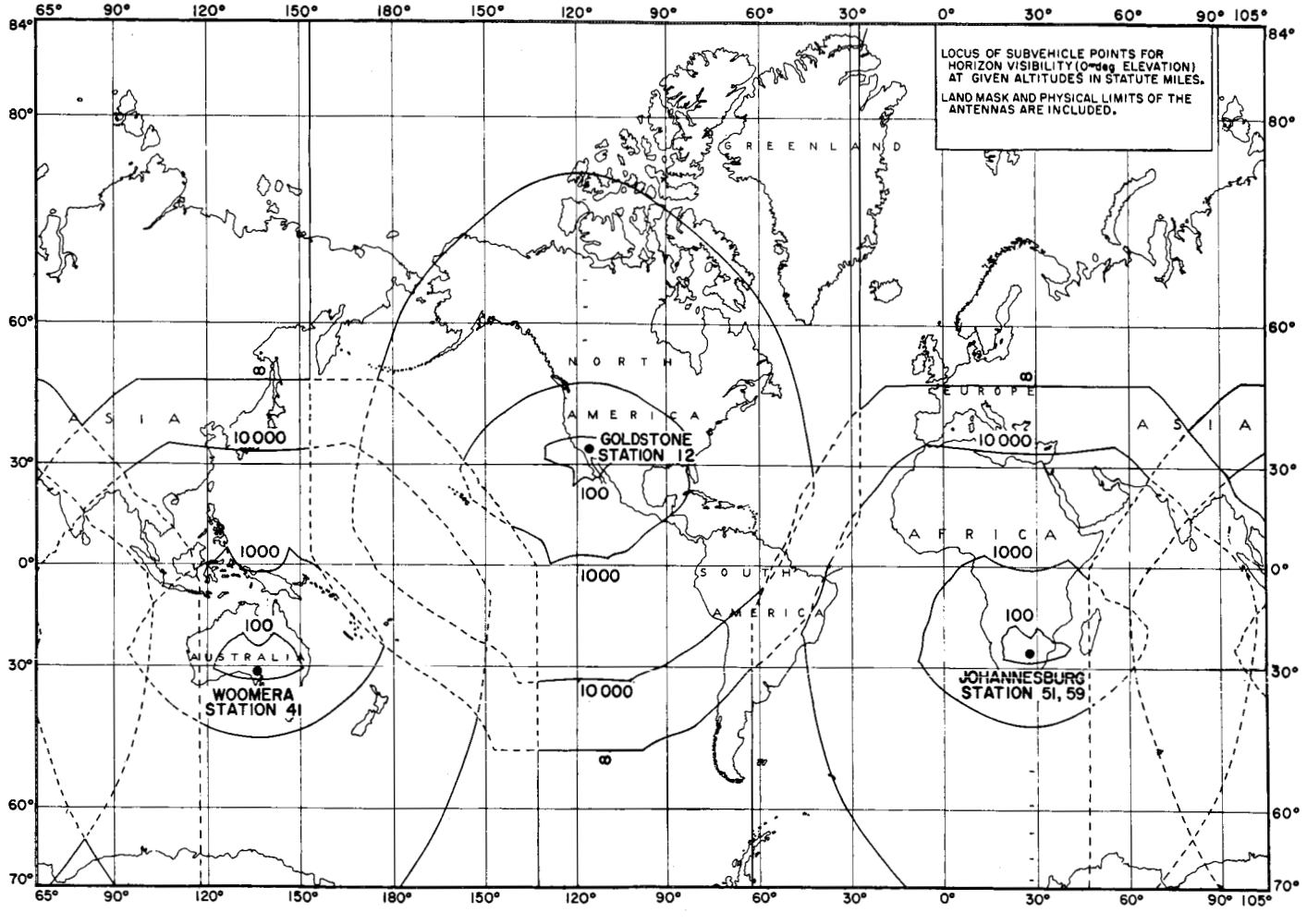

Fig. 18. Station coverage for 85-ft-diameter polar mount DSIF antenna (Goldstone, Woomera, Johannesburg)

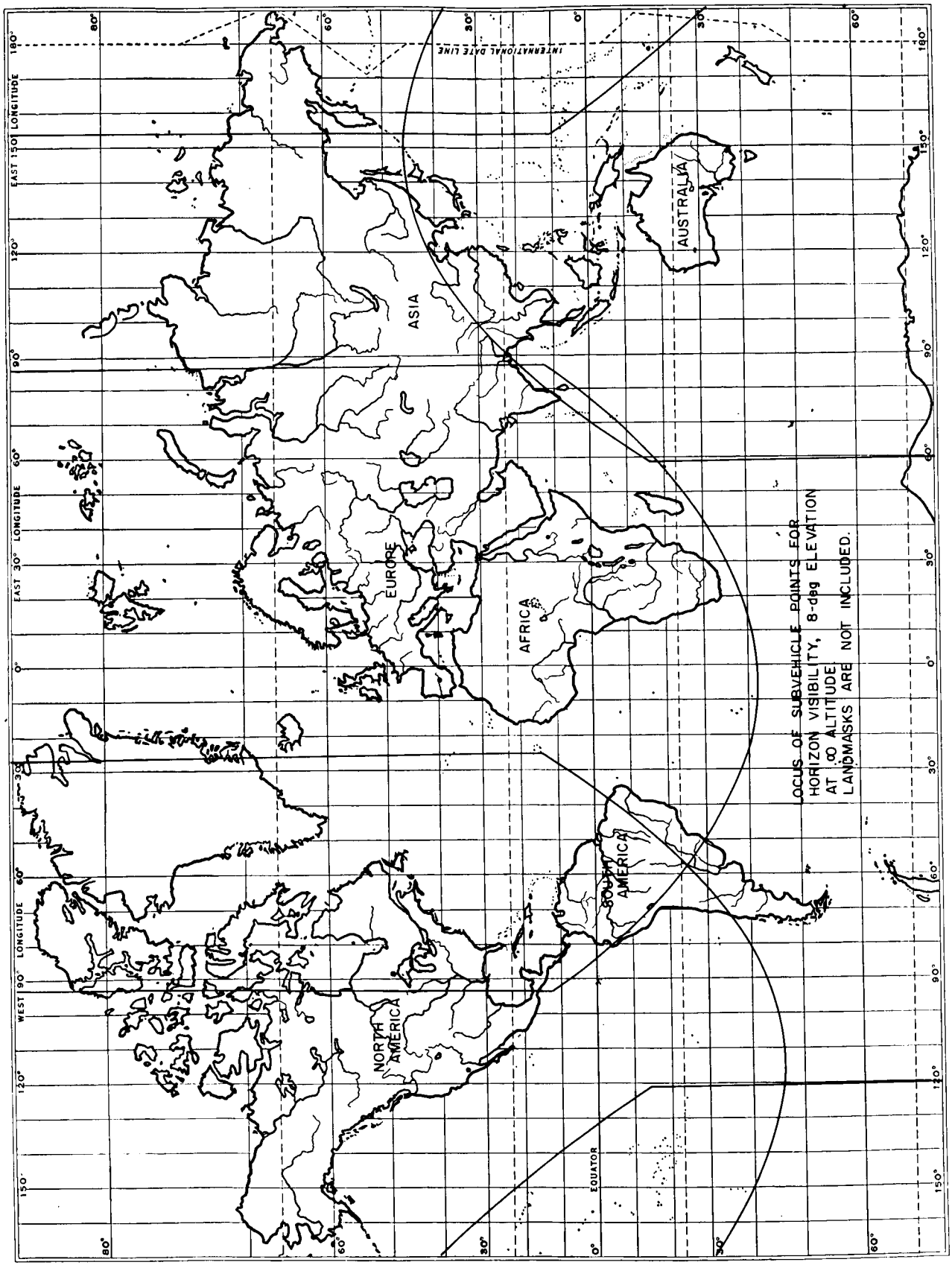

Fig. 19. Station coverage for 85-ft-diameter polar mount DSIF antenna (Goldstone, Madrid, Canberra)

X. DEEP SPACE INSTRUMENTATION FACILITY SYSTEM CAPABILITIES[21]

A. Angle Tracking

The automatic angle tracking systems used in the DSIF are of the simultaneous-lobing type. The 85-ft HA-Dec antennas (I)[22] have two maximum tracking rate capabilities, 0.7 deg/sec and 0.03 deg/sec about each axis, depending on tracking system bandwidth requirements. During the periods in which angle tracking accuracy is most significant (e.g., when data for an initial ephemeris calculation are required), the strong signal levels available result in a root-mean-square angle-tracking error from 0.01 to 0.02 deg. The rms tracking error at receiver threshold increases to approximately 0.05 deg. Bias errors lie in the range of −0.1 to +0.1 deg. However, optical calibration techniques such as star tracking have led to the accurate determination of certain bias errrors, and these are removed from the observed data at the computational facility. Resolution of the angle encoders is 0.002 deg.

The 85-ft Az-El mount antenna, which is located at the Goldstone (Venus) site, is used primarily in engineering and development work for the DSIF. However, in emergencies, or where special equipment installed on this antenna is required, this station may be used in DSIF operations. An example of this is the planned use of the 100-kw transmitter, which is installed on the 85-ft antenna at the Venus site, in operations with the *Mariner* spacecraft which is scheduled to pass by the planet Mars in 1965. This antenna is capable of tracking rates up to 2.0 deg/sec and has rms tracking errors comparable to the polar-mount 85-ft antennas.

Angle data from all the DSIF antennas are digitally encoded by angle sensors on the antenna, and the coded signals are recorded in teletype code on punched paper tape by the data handling equipment.

B. Doppler

One- and two-way doppler measurement capability is included at all stations in the DSIF. Two-way doppler requires a ground transmitter in the vicinity of the DSIF receiver to achieve frequency control by a single exciter. The distance at which the DSIF stations can obtain doppler data is, of course, dependent on the sensitivity of the spacecraft receiver and the power output of the spacecraft transponder; if the carrier can be tracked in phase, doppler data can be made available.

The accuracy of one-way doppler data is limited primarily by the average frequency instability of the spacecraft oscillator. The detected doppler in either the one- or two-way system is equal to the doppler shift at the received RF frequency with the addition of a 1-Mc bias. The 1-Mc bias is derived from the station's ultrastable oscillator.

Doppler frequency data are obtained by use of digital frequency counters whose basic timing frequency is obtained from the station's ultrastable oscillator. The available counting intervals and sampling rates are shown in Table 8. Two counters are used in any one of three different modes as follows:

Mode 1. Either counter (or both in parallel) counts the doppler frequency for a specific counting interval (always less than the sampling rate); the count is read out and then reset to zero and the process repeated.

Table 8. Data system sampling rates and doppler counting intervals

Available sampling rates		Available doppler counting intervals
1 sec	1 min	1 sec
2	2	5
3	3	10
4	4	20
5	5	30
6	6	40
7	7	50
8	8	60
9	9	continuous
10	10	
20	20	
30	30	
40	40	
50	50	
60	60	
70	70	
80	80	
90	90	

[21]The material in this section was adapted from Ref. 9.

[22]Throughout this section the following code is employed: (I) designates existing and installed facilities; (A) designates authorized and funded projects; (P) designates proposed but not yet funded projects.

Mode 2. Same as Mode 1 except the counters count alternately. In this case, the counting interval can be equal to or less than the sample rate. When the sample rate and counting interval are equal, the sum of the readings of both counters is equivalent to a continuous count.

Mode 3. One counter counts continuously while the other counter acts as a storage register to hold the sampled reading while the reading is read out. The reading rate is controlled by the sample rate, and the register counter is reset to zero after readout. The actual data are an accumulative count until lock is broken.

The first two modes are "destruct" modes, while the third mode is a "continuous" mode and provides a direct measurement of the change in range over the time interval.

There are also two more options in the data sampling system which are planned to become available to the user. They are (1) the ability to count every zero crossing rather than just positive-going zero crossings (i.e., ½ cycle count) and (2) the ability to use a suitable multiplier on the doppler (i.e., the frequency is multiplied up so that more zero crossings are counted per unit of time). These options should be used with careful planning so that data errors can be minimized and all real information in the data can be extracted. Sections IV and V discussed some of the items which should be considered.

C. Precision Ranging

A ranging system is presently under development by JPL and is planned for installation at the different stations when the S-band equipment is installed (see Table 7). The system measures the time difference between two identical, separately generated, pseudo-random noise codes (one generated at the transmitter for modulation, and the other generated at the receiver for correlation detection) to represent range. The transponder in the spacecraft receives the code-modulated transmitted signal and retransmits the same modulation back to the ground. The transponder is called a "turn-around" transponder, and normal signal-to-noise ratios available with this type of system limit the measurement of range to less than 800,000 km. The resolution of the ranging system is 0.007 μsec round-trip time, which is approximately equivalent to 1.05 meters one way. However, worst-case estimates of the unknown time delays in the receiving system are expected to limit the accuracy of the ranging system to ± 0.1 μsec round-trip time, which is approximately equivalent to ± 15 meters one way.

The ranging system is operable as long as carrier phase coherence is maintained in the two-way system. The general mode of operation will be to initiate range modulation, establish range lock, and then remove range modulation and count carrier doppler cycles to maintain a range tally.

It is possible to extend this method of ranging to planetary distances by equipping the spacecraft transponder with the same type of pseudorandom code generator, which reconstructs the code before retransmission to the Earth. Such a system has been designed and built, and will be installed at Goldstone whenever there is a project requirement. It is not considered necesssary at this time to equip each longitude with this capability.

D. Tracking-Data Handling

Tracking-data handling equipment is operational at all Deep Space Stations. This equipment automatically punches out, on paper tape and in standard Baudot teleprinter five-hole code, characters which represent carriage return, line feed, figures, spaces, and the following technical information:

Station identification number
Spacecraft identification number
Data condition
Greenwich Mean Time (GMT)
Antenna hour or azimuth angle
Antenna declination or elevation angle
Doppler frequency
Range data including "range condition" code (A)
Transmitter frequency (A)
Day of year

The format is so designed that one complete set of information is printed on one or two lines of a teleprinter page printer, which will accept a nominal 60 characters per line, including spaces.

A complete line (or two lines) of information is called a data sample and the rate at which these samples are read out is determined by the settings of the sampling rate switches (see Table 8). The system is capable of punching at a rate of 60 characters per sec, using two punches connected to operate singly or in parallel. A

control is available so that both punches can operate in parallel but with one punch set to punch at 1/1, 1/2, 1/3, 1/4, 1/5, 1/6, 1/7, 1/8, 1/9, or 1/10 the rate of the other punch. Since the normal maximum teletype speed is 6 characters per sec (60 words per min), it is possible to use one punch to punch out data for real-time teleprinter transmission while the other punch is punching out data at the maximum rate. The rate of tracking-data sampling is generally determined by project requirements and varies considerably over the period of a mission.

REFERENCES

1. Deep Space Network *Commitment Document for the Lunar Orbiter Project,* EPD 243, Jet Propulsion Laboratory, Pasadena, Calif., December 19, 1964.
2. *Lunar Orbiter Project Support Instrumentation Requirements Document (SIRD)* (Revision 3), Lunar Orbiter Project Office, Langley Research Center, NASA, Langley Station, Hampton, Va., October 12, 1964.
3. *Further Discussion of Selenodetic Tracking Requirements in the SIRD,* letter dated February 4, 1965, from M. S. Johnson, Manager, Deep Space Network, to C. H. Nelson, Manager, Lunar Orbiter Project, Langley Research Center, Hampton, Va., Attention: W. J. Boyer.
4. Trask, D. W., et al., *DSIF Accuracy Projection and Lunar Mission Capability,* Technical Report No. 32-768, Jet Propulsion Laboratory, Pasadena, Calif., May 31, 1965.
5. Holzman, R. E., *Users' Guide to the Tracking Data Processor and Orbit Data Generator Programs,* Reorder No. 65-205, Jet Propulsion Laboratory, Pasadena, Calif., May 14, 1965.
6. Warner, M. R., and Nead, M. W., *SPODP — Single Precision Orbit Determination Program,* Technical Memorandum No. 33-204, Jet Propulsion Laboratory, Pasadena, Calif., February 15, 1965.
7. Epstein, H., *Ranger 7 — Doppler Ranger Residues,* Apollo Note No. 265, Bisset-Berman Corp., Santa Monica, Calif., October 7, 1964.
8. Sjogren, W. L., et al., *The Ranger VI Flight Path and Its Determination from Tracking Data,* Technical Report No. 32-605, Jet Propulsion Laboratory, Pasadena, Calif., December 15, 1964.
9. *System Capabilities and Development Schedule of the Deep Space Instrumentation Facility 1964-68* (Revision 1), Technical Memorandum No. 33-83, Jet Propulsion Laboratory, Pasadena, Calif., April 24, 1964.
10. Wollenhaupt, W. R., et al., *Ranger VII Flight Path and Its Determination from Tracking Data,* Technical Report No. 32-694, Jet Propulsion Laboratory, Pasadena, Calif., December 15, 1964.

JET PROPULSION LABORATORY *California Institute of Technology • 4800 Oak Grove Drive, Pasadena, California 91103*

Recipients of Jet Propulsion Laboratory
Technical Memorandum No. 33-230

SUBJECT: Errata for TM 33-230

Gentlemen:

It is requested that the following errors be corrected in your copy of Jet Propulsion Laboratory Technical Memorandum No. 33-230 entitled, *Characteristics and Format of the Tracking Data to be Obtained by the NASA Deep Space Instrumentation Facility for Lunar Orbiter*, by J. Lorell, J. D. Anderson, and W. L. Sjogren, dated June 15, 1965:

Page 5, line 11 of footnote 10: *for* effective *read* effect

Page 9, left column, line 8: *for* $K_2 = 0.025$ cps$^{1/2}$ *read* $K_2 = 0.025$ cyc/sec$^{1/2}$

Page 9, left column, line 10: *for* $K_3 = 0.49$ cps *read* $K_3 = 0.49$ cyc

Page 12, figure caption: *for* Ranger VI *read* Ranger VII

Page 22, Eq. (7-6): *for* $+\frac{1}{2}\left[\dot{R}(t;\,rec)\cdot\dot{R}(t;\,rec) - \dot{R}(t_{tr};\,tr)\cdot\dot{R}(t_{tr};\,tr)\right]$

read $+\frac{1}{2}\left[\dot{\mathbf{R}}(t;\,rec)\cdot\dot{\mathbf{R}}(t;\,rec) - \dot{\mathbf{R}}(t_{tr};\,tr)\cdot\dot{\mathbf{R}}(t_{tr};\,tr)\right]$

Page 22, left column, line 8: *for* $r(t_p)$ *read* $\mathbf{r}(t_p)$

Page 22, Eq. (7-7): *for* $= \left[r(tp) - \mathbf{R}(t_{tr};\,tr)\right]\cdot\left[r(tp) - \mathbf{R}(t_{tr};\,tr)\right]$

read $= \left[\mathbf{r}(t_p) - \mathbf{R}(t_{tr};\,tr)\right]\cdot\left[\mathbf{r}(t_p) - \mathbf{R}(t_{tr};\,tr)\right]$

Page 22, Eq. (7-8): *for* $= \left[r(tp) - \mathbf{R}(t_{tr};\,tr)\right]\cdot\left[r(tp) - \dot{\mathbf{R}}(t_{tr};\,tr)\right]$

read $= \left[\mathbf{r}(t_p) - \mathbf{R}(t_{tr};\,tr)\right]\cdot\left[\dot{\mathbf{r}}(t_p) - \dot{\mathbf{R}}(t_{tr};\,tr)\right]$

Page 22, left column, line 13 from bottom: *for* ν_{ob}/ω_{4tr} *read* $\nu_{ob}/\omega_4\nu_{tr}$

Page 22, left column, line 7 from bottom: *for* $F(t)$ *read* $\ddot{F}(t)$

Page 22, Eq. (7-9): *for* $\rho(t_{ob})$ *read* $\dddot{\rho}(t_{ob})$

Very truly yours,

for I. E. Newlan, *Manager*
Technical Information Section

Telephone 354-4321

Twx 213-449-2451